AIAA SciTech Forum
12-16 January 2026, Orlando, FL
AIAA SCITECH 2026 Forum

10.2514/6.2026-0108

Duality between Incremental Nonlinear Dynamic Inversion and Transformation-based Quasi-Linear Parameter-Varying Control

Tijmen Pollack*, Spilios Theodoulis†, and Xuerui Wang‡
Delft University of Technology, 2629HS Delft, The Netherlands

This paper presents a transformation-based robust nonlinear control design framework based on the concepts of Incremental Nonlinear Dynamic Inversion (INDI) and quasi-Linear Parameter-Varying (q-LPV) control. The duality between these popular control design paradigms is investigated. Control-oriented q-LPV model representations of (I)NDI-based closed-loop systems are presented for various inversion strategies, which creates a basis for robust synthesis and analysis of (I)NDI-based designs in the LPV sense. This includes extensions to singular perturbations that limit exact inversion in reality. The presented approach is demonstrated in a design case study for a nonlinear aeroservoelastic system, where INDI-based controllers are synthesized and quantitatively compared with direct q-LPV control based on linear fractional transformations.

I. Introduction

One of the key challenges in robust control design is to ensure adequate performance in the presence of uncertainty within the limitations posed by physical hardware. This relates to stability, performance, and control activity in the context of both dynamic and parametric uncertainty. In this context, $\mathcal{H}_\infty$ theory is foundational to obtaining important robustness guarantees within the class of Linear Time-Invariant (LTI) systems [1–3]. As such, it can be used to evaluate or generate LTI controllers that inherit such properties automatically. Frameworks such as μ-synthesis [3] and Integral Quadratic Constraints (IQCs) [4, 5] represent powerful extensions of the basic theory that allow designers to tackle a wide variety of control problems.

However, in spite of these guarantees, LTI control design generally captures only a part of the full control design problem. Real-world physical systems are generally nonlinear and time-varying. Consequently, LTI models only represent local approximations of the plant dynamics around selected operating points. Therefore, a classical approach is to perform interpolation-based gain scheduling of local LTI controllers to cover the full operating domain of the system [6–8]. This procedure can lead to effective designs that preserve the input-output characteristics of the family of linearized closed-loop systems [9, 10] and thereby retain crucial LTI robustness guarantees. However, a fundamental limitation of this approach lies in the fact that no guarantees are obtained *a-priori* with respect to nonlinear stability and performance [11, 12]. This implies that the designer cannot be confident about these aspects without additional verification. Some design guidelines do exist to alleviate this issue: for example, good behavior can often be expected if the scheduling parameter varies slowly [12] and if smooth interpolation of control gains is performed [13]. Nevertheless, additional analysis is still needed, which is often done based on an extensive number of Monte Carlo simulations. This implies that a considerable number of design iterations may be required to ensure compliance with all objectives.

To make nonlinear robust control design more efficient, a framework is desired that provides a-priori theoretical guarantees similar to those provided for LTI systems by $\mathcal{H}_\infty$-theory. The class of Linear Parameter-Varying (LPV) [14] systems forms an important concept herein. LPV systems are natural extensions of their LTI counterparts, where the state-space matrices are functions of time-varying scheduling parameters. Within this framework, important quadratic stability and performance guarantees can be obtained [15–17]. However, before LPV-based controller design can be performed, the original nonlinear and time-varying system dynamics should be captured in the LPV form. This process is known as LPV modeling. Several LPV modeling approaches exist [18, 19], including Jacobian linearization, State Transformation (ST) [20], and Function Substitution (FS) [21]. In essence, these aim to *embed* [22] the original system dynamics into an LPV representation.

Special attention is required for those systems where the scheduling variable is a function of the open-loop system state. These are known as *quasi*-LPV (q-LPV) systems. The ST approach was proposed by Shamma and Cloutier [20] to

*Postdoctoral Researcher, Aerospace Structures and Materials Section, Faculty of Aerospace Engineering.
†Associate Professor, Control & Simulation Section, Faculty of Aerospace Engineering, AIAA Associate Fellow.
‡Assistant Professor, Control & Simulation / Aerospace Structures and Materials, Faculty of Aerospace Engineering, AIAA Senior Member.

construct such q-LPV descriptions for the important class of output-nonlinear systems. Through a transformation of the state equation, this strategy aims to "remove" plant nonlinearities [18] without any intermediate approximations. The resulting q-LPV model enables the use of a wide range of LPV synthesis and analysis methods. Consequently, it can be used to obtain nonlinear control designs in accordance with well-established robust control design principles. The technique has been used successfully in several studies and applications [20, 23–26], which exemplifies its effectiveness.

From a broader perspective, the notion of transforming plant dynamics through a "cancellation" of nonlinearities as in ST-based q-LPV modeling is conceptually analogous to the principle of *feedback linearization*. This connection has been raised in a number of publications [20, 27]. In the aerospace community, feedback linearization is also known as Nonlinear Dynamic Inversion (NDI) [28]. The objective of NDI is to transform the closed-loop input-output dynamics associated with the selected controlled variables (CVs) into a chain of ideal integrators. This *inversion* step is achieved in an on-line fashion through a combination of feedback and an embedded model representation of the physical plant. Since the related transformation step forms an explicit part of the controller, the NDI technique imposes a particular structure on the control design. This structure brings a degree of modularity and transparency that can be beneficial during control law development [29]. Consequently, NDI-based design is a popular technique for aerospace applications that has been shown to perform successfully on many occasions (e.g., [30–32]). However, in spite of its benefits, the particular structure of NDI-based controllers may have important robustness implications.

First, the fact that NDI depends on the availability of an accurate model representation has been a subject of significant concern. Consequently, there has been a widespread interest in alternative design approaches that reduce the dependence on this model. The concept of *sensor-based* Incremental Nonlinear Dynamic Inversion (INDI) [33] has become of significance here. With this strategy, a substantial part of the model is omitted by using direct sensor feedback. As a result, the sensor-based method has improved robustness to regular perturbations compared to the classical variant [34]. However, this characteristic comes at the expense of reduced robustness to unknown singular perturbations caused by unmodeled higher-order dynamics (e.g., flexible modes and sensor delays) that typically arise in practice [35]. The concept of *hybrid* INDI has been proposed [36–38] to enable a better balance of these robustness properties. With this method, model-based and sensor-based inversion signals are blended to perform inversion error compensation within a desired bandwidth. This enables the designer to improve robustness within the INDI structure.

A second factor of concern relates to the linearization property of NDI and INDI, briefly summarized as (I)NDI from hereon, in a general sense. This relates to the fundamental nature of the (I)NDI framework as a whole and is therefore irrespective of the selected inversion strategy (i.e., model-based, sensor-based, or hybrid). As suggested by [20], dynamic inversion-based transformation does not reflect typical robust design principles. For example, regulation and tracking are often required only within a finite bandwidth. This contrasts with the inversion loop, which aims to linearize the system dynamics across all frequencies. At the same time, exact inversion is seldom possible due to the presence of higher-order dynamics (e.g., due to actuators, sensors, filters, and unmodeled dynamics). This results in *inversion distortions* [29], which undermine the linearization property and obscure the process of obtaining guarantees.

Based on this discussion, it can be seen that the robustness implications of (I)NDI require adequate consideration. Immediate deployment of (I)NDI-controlled systems without thorough robust stability analysis can therefore lead to unexpected and undesirable situations. In this light, additional instruments are necessary to obtain important robustness guarantees. It was shown in [35, 38] how $\mathcal{H}_\infty$ design techniques can be used to synthesize robust (I)NDI controllers in a divide-and-conquer LTI sense while preserving their nonlinear nature. Moreover, [39] demonstrated how ST-based q-LPV modeling can be leveraged to analyze nonlinear stability and performance properties of locally optimized model-based and hybrid (I)NDI controllers. In effect, this work established a first link between the INDI and q-LPV control frameworks. This link forms an important basis for better understanding the fundamental robustness implications of INDI-based control mentioned above, which leads to the contributions of the present work.

In brief, the aim of this paper is to develop a deeper understanding of the robustness properties of INDI-based controllers in a q-LPV context. In doing so, the synergies between the q-LPV ST approach and the (I)NDI framework will be revealed. It will be shown how this relates to the formulation of q-LPV models for (I)NDI-controlled nonlinear systems of different types. The range of *inversion strategies* mentioned before will be covered herein. This not only includes the model-based and hybrid variants as previously considered in [39], but also covers the sensor-based strategy in the filtered form. The presented q-LPV model framework is used in an example case study in which LPV synthesis of INDI-based controllers is performed for a prototypical nonlinear aeroservoelastic system. To this end, a non-smooth $\mathcal{H}_\infty$ synthesis scheme is established for structured LPV controllers in Linear Fractional Transformational (LFT) form. The resulting INDI designs are compared to a direct LFT-based q-LPV controller that is of the same order but remains unstructured otherwise. This provides quantitative insights into the robustness implications of the inversion strategy and transformation concepts for the presented design scenario.

In summary, the paper has the following contributions:

1) A methodological comparison of ST-based q-LPV and (I)NDI as transformation-based control schemes;
2) General q-LPV model formulations for model-based, sensor-based, and hybrid (I)NDI-based control laws, including explicit incorporation of singular perturbations;
3) Application of non-smooth $\mathcal{H}_\infty$ synthesis to INDI control laws represented as structured q-LPV controllers.
4) Demonstration of the proposed framework to robust stabilization of a nonlinear aeroservoelastic system.

These contributions are useful not only to the INDI and broader feedback linearization communities but also provide new insights into the implications of plant transformations in q-LPV design in general. In particular, the presented framework enables quantitative comparisons between (I)NDI-based and direct q-LPV controllers. These insights are broadly applicable to any nonlinear dynamic system that can be captured in the output-nonlinear form and are not limited to the example case study presented herein.

The paper outline is as follows. Section II first covers theoretical background for (I)NDI-based control design and LPV systems. Quasi-LPV model formulations for (I)NDI-based control laws are presented in Section III, together with a discussion of the robustness implications of plant transformations. The structured LPV synthesis approach is elaborated upon in Section IV. The aeroservoelastic design case study is described in Section V, together with a presentation of the main results and a discussion of the implications. Section VI concludes the article. Finally, additional derivations can be found in Appendix A.

II. Theoretical Fundamentals

This section briefly reviews the fundamentals of Incremental Nonlinear Dynamic Inversion (INDI) control and Linear-Parameter Varying (LPV) systems theory.

A. Incremental Nonlinear Dynamic Inversion

Incremental Nonlinear Dynamic Inversion (INDI) aims to address several of the limitations of the classical Nonlinear Dynamic Inversion (NDI) approach, which is also known as feedback linearization in the wider control community. Accordingly, the basic principles of feedback linearization are discussed first. This is followed by a derivation of the incremental form and a discussion of the role of different inversion strategies.

1. Feedback linearization

The concept of feedback linearization aims at transforming nonlinear plants in the sense of input-output or full-state linearization through diffeomorphic state transformations and feedback. This applies to square, input-affine systems of the form

$$\begin{cases} \dot{\boldsymbol{x}} = \boldsymbol{f}(\boldsymbol{x}) + \boldsymbol{G}(\boldsymbol{x})\boldsymbol{u} \\ \boldsymbol{y} = \boldsymbol{h}(\boldsymbol{x}) \end{cases} \tag{1}$$

which consists of the state vector $\boldsymbol{x} \in \mathbb{R}^n$, the input vector $\boldsymbol{u} \in \mathbb{R}^m$, the controlled variable (CV) vector $\boldsymbol{y} \in \mathbb{R}^m$, and smooth mappings $\boldsymbol{f}$, $\boldsymbol{G}$, and $\boldsymbol{h}$. A partial change of coordinates is performed by taking repeated time derivatives of $\boldsymbol{y}$ until the control input $\boldsymbol{u}$ appears explicitly:

$$\begin{aligned} \boldsymbol{y}^{(\boldsymbol{r})} &= \begin{bmatrix} \mathcal{L}_f^{r_1} h_1(\boldsymbol{x}) \\ \vdots \\ \mathcal{L}_f^{r_m} h_m(\boldsymbol{x}) \end{bmatrix} + \begin{bmatrix} \mathcal{L}_{g_1}\mathcal{L}_f^{r_1-1} h_1(\boldsymbol{x}) & \dots & \mathcal{L}_{g_m}\mathcal{L}_f^{r_1-1} h_1(\boldsymbol{x}) \\ \vdots & \ddots & \vdots \\ \mathcal{L}_{g_1}\mathcal{L}_f^{r_m-1} h_m(\boldsymbol{x}) & \dots & \mathcal{L}_{g_m}\mathcal{L}_f^{r_m-1} h_m(\boldsymbol{x}) \end{bmatrix} \boldsymbol{u} \\ &\triangleq \boldsymbol{\alpha}(\boldsymbol{x}) + \mathcal{B}(\boldsymbol{x})\boldsymbol{u} \end{aligned} \tag{2}$$

Here, $\mathcal{L}_f^k h_i(\boldsymbol{x})$ and $\mathcal{L}_{g_i}\mathcal{L}_f^k h_i(\boldsymbol{x})$ represent the Lie derivatives of the function h_i along the vectors fields $\boldsymbol{f}$ and $\boldsymbol{g_i}$ [40]. Moreover, $\boldsymbol{r}$ is referred to as the system *relative degree*. If some function $\boldsymbol{h}$ exists such that $\|\boldsymbol{r}\|_1 = r = n$, the system is said to be full-state feedback linearizable [40]. Otherwise, the system can be partially linearized at most. In this scenario, a second change of variables is required for the states that cannot be observed through $\boldsymbol{y}$. This leads to the definition of the *normal form*, which is obtained through the combined coordinate transformation $\begin{bmatrix} \boldsymbol{\xi}^T & \boldsymbol{\eta}^T \end{bmatrix}^T = T(\boldsymbol{x})$ [40]:

$$\begin{aligned}\dot{\boldsymbol{\xi}} &= A_c\boldsymbol{\xi} + B_c\left[\boldsymbol{\alpha}(\boldsymbol{x}) + \mathcal{B}(\boldsymbol{x})\boldsymbol{u}\right]\\ \dot{\boldsymbol{\eta}} &= \boldsymbol{f}_0(\boldsymbol{\eta},\boldsymbol{\xi})\\ \boldsymbol{y} &= C_c\boldsymbol{\xi}\end{aligned} \tag{3}$$

Note that the normal form requires the origin $\boldsymbol{\xi} = \boldsymbol{\eta} = \boldsymbol{0}$ to be an equilibrium point [40]. Consequently, the control law

$$\boldsymbol{u} = \hat{\mathcal{B}}^{-1}(\boldsymbol{x})\left[\boldsymbol{\nu} - \hat{\boldsymbol{\alpha}}(\boldsymbol{x})\right] \tag{4}$$

serves to transform the dynamics in $\boldsymbol{\xi}$ to a chain of ideal integrators. Here, $\hat{\boldsymbol{\alpha}}(\boldsymbol{x})$ and $\hat{\mathcal{B}}(\boldsymbol{x})$ represent model representations of $\boldsymbol{\alpha}(\boldsymbol{x})$ and $\mathcal{B}(\boldsymbol{x})$, respectively, and $\boldsymbol{\nu} \in \mathbb{R}^m$ is the pseudo-control vector generated by an auxiliary stabilizing control law. The resulting transformed system takes the form of:

$$\begin{aligned}\dot{\boldsymbol{\xi}} &= A_c\boldsymbol{\xi} + B_c\boldsymbol{\nu}\\ \dot{\boldsymbol{\eta}} &= \boldsymbol{f}_0(\boldsymbol{\eta},\boldsymbol{\xi})\\ \boldsymbol{y} &= C_c\boldsymbol{\xi}\end{aligned} \tag{5}$$

Global asymptotic stability with respect to the origin requires the *zero dynamics* $\dot{\boldsymbol{\eta}} = \boldsymbol{f}_0(\boldsymbol{\eta},\boldsymbol{0})$ to be stable, which is influenced by the choice of the CV. Additional analysis may be required to verify this [28]. Consequently, the zero dynamics play a fundamental role in the behavior of the overall closed-loop system. For additional details on feedback linearization, the reader may refer to [40].

2. Alternative inversion strategies

With regards to the standard feedback linearization framework, several fundamental limitations can be identified. This includes, but is not limited to, the affine system assumption and the need for accurate models to perform the linearization step. To this end, the INDI framework has been proposed [34]. The incremental formulation aims to remove the affine system limitation and enables the reduction of controller model dependency. It is based on taking the Taylor expansion of the output dynamics around the previous time step (indicated by the subscript $|_0$) as follows:

$$\boldsymbol{y}^{(\boldsymbol{r})} = \boldsymbol{y}_0^{(\boldsymbol{r})} + \left.\frac{\partial\left[\boldsymbol{\alpha}(\boldsymbol{x}) + \mathcal{B}(\boldsymbol{x},\boldsymbol{u})\right]}{\partial\boldsymbol{x}}\right|_0 \underbrace{(\boldsymbol{x} - \boldsymbol{x}_0)}_{\Delta\boldsymbol{x}} + \left.\frac{\partial\mathcal{B}(\boldsymbol{x},\boldsymbol{u})}{\partial\boldsymbol{u}}\right|_0 \underbrace{(\boldsymbol{u} - \boldsymbol{u}_0)}_{\Delta\boldsymbol{u}} + \boldsymbol{R}_1 \tag{6}$$

where $\boldsymbol{R}_1$ represents the higher order terms. Then, the following incremental control law is constructed:

$$\boldsymbol{u} = \boldsymbol{u}_0 + \hat{\mathcal{B}}^{-1}(\boldsymbol{x}_0,\boldsymbol{u}_0)\left[\boldsymbol{\nu} - \boldsymbol{y}_0^{(\boldsymbol{r})}\right] \tag{7}$$

It can be seen that the dependency of the control law on $\boldsymbol{\alpha}(\boldsymbol{x})$ can be completely removed if direct feedback of $\boldsymbol{u}_0$ and $\boldsymbol{y}_0^{(\boldsymbol{r})}$ is used. This greatly enhances robustness to regular perturbations [34] and is commonly referred to as *sensor-based* INDI. The terminology emphasizes the difference from the classical case presented before, which is referred to as *model-based*. Therefore, various *inversion strategies* can be adopted to perform feedback linearization.

The connection between the inversion strategy and robustness requires careful consideration. In this light, a robust control design needs to have balanced robustness characteristics against a mix of different uncertainties. For example, the improved robustness against regular perturbations generally comes at the expense of robustness against unknown singular perturbations associated with high-order dynamic uncertainties [35]. The need for systematic robustness trade-offs forms the motivation for *hybrid* INDI [38]. Using the following scheme, this approach takes advantage of both model-based and sensor-based estimations of $\boldsymbol{y}_0^{(\boldsymbol{r})}$ as complementary sources of information:

$$\hat{\boldsymbol{y}}_{0,HB}^{(\boldsymbol{r})} = (I - K_cH_c)\,\hat{\boldsymbol{y}}_{0,MB}^{(\boldsymbol{r})} + K_cH_c\hat{\boldsymbol{y}}_{0,SB}^{(\boldsymbol{r})} \tag{8}$$

Here, the compensation gain $K_c \in [0,1]$ and filter H_c enable a blending of model-based and sensor-based prediction signals across frequency. This can be achieved using a scaled complementary filter (SCF) implementation [38]. In effect, this blending results in a compensation of model-based inversion errors. To illustrate this, consider the case where the output dynamics are affected by parametric model uncertainty and an exogenous disturbance signal $\boldsymbol{d}$:

$$\hat{\boldsymbol{y}}_{0,HB}^{(\boldsymbol{r})} = (I - K_cH_c)\underbrace{\left[\hat{\boldsymbol{\alpha}}(\hat{\boldsymbol{x}}_0) + \hat{\mathcal{B}}(\hat{\boldsymbol{x}}_0,\boldsymbol{u}_0)\right)}_{\hat{\boldsymbol{y}}_{0,MB}^{(\boldsymbol{r})}} + K_cH_c\underbrace{\left[\boldsymbol{\alpha}(\boldsymbol{x}_0) + \mathcal{B}(\boldsymbol{x}_0,\boldsymbol{u}_0) + \boldsymbol{d}_0\right]}_{\boldsymbol{y}_{0,SB}^{(\boldsymbol{r})}} \tag{9}$$

Then, taking $\hat{\mathcal{B}}(\hat{\boldsymbol{x}}_0, \boldsymbol{u}_0) = \mathcal{B}(\boldsymbol{x}_0, \boldsymbol{u}_0)$ for the purpose of illustration and reordering terms:

$$\begin{aligned}\hat{\boldsymbol{y}}^{(\boldsymbol{r})}_{0,HB} &= \left[\hat{\boldsymbol{\alpha}}(\hat{\boldsymbol{x}}_0) + \mathcal{B}(\boldsymbol{x}_0, \boldsymbol{u}_0)\right] + K_c H_c \left[\boldsymbol{\alpha}(\boldsymbol{x}_0) - \hat{\boldsymbol{\alpha}}(\hat{\boldsymbol{x}}_0) + \boldsymbol{d}_0\right] \\ &\triangleq \hat{\boldsymbol{y}}^{(\boldsymbol{r})}_{0,MB} + K_c H_c \boldsymbol{e}_{\boldsymbol{\xi},0}\end{aligned} \tag{10}$$

The SCF parameters (K_c and H_c) represent tunable elements that determine the equivalent gain and bandwidth associated with the inversion strategy [38]. Note that in the absence of uncertainty and disturbances, i.e., when $\boldsymbol{e}_{\boldsymbol{\xi}} = \boldsymbol{0}$, the inversion is not affected by these parameters.

B. Linear Parameter-Varying Systems

The Linear Parameter-Varying (LPV) system framework represents an *ensemble* of modeling techniques and design representations. Consequently, there are many theories and concepts that fall under this category. In this section, some elementary background is provided first. This is followed by an introduction to the State Transformation (ST) technique proposed by Shamma and Cloutier [20] for quasi-LPV system modeling.

1. Background

LPV systems relate to a class of systems where the state space matrices are a continuous function of a generally time-varying, exogenous scheduling parameter $\boldsymbol{\rho} : \mathbb{R}^{n_\rho} \rightarrow \mathcal{P}$. Its definition takes the form of:

$$\begin{bmatrix}\dot{\boldsymbol{x}}(t) \\ \boldsymbol{y}(t)\end{bmatrix} = \begin{bmatrix}A(\boldsymbol{\rho}(t)) & B(\boldsymbol{\rho}(t)) \\ C(\boldsymbol{\rho}(t)) & D(\boldsymbol{\rho}(t))\end{bmatrix}\begin{bmatrix}\boldsymbol{x}(t) \\ \boldsymbol{u}(t)\end{bmatrix} \tag{11}$$

Typically, the scheduling parameter is assumed a-priori to be bounded in terms of magnitude. Similar bounds on the rate-of-variation $-\beta_i \leq \dot{\rho}_i(t) \leq \beta_i$ can also be considered. Although many systems may lead to representations of the above form, care is required in terms of any interpretations that follow. For example, whereas a family of LTI systems obtained through Jacobian linearization may take the same form, performing LPV-based analysis based on this type of modeling approach may lead to misleading results with respect to the original nonlinear system. This shows the importance of the underlying modeling strategy. For further discussion on this aspect, the reader may refer to [6, 7].

2. Shamma's State Transformation

Given this background, an LPV modeling strategy that closely relates to the original nonlinear system is desired. This leads to the ST approach proposed by Shamma and Cloutier [20]. It considers square, nonlinear, input-affine systems of the form

$$\begin{bmatrix}\dot{\boldsymbol{z}} \\ \dot{\boldsymbol{w}}\end{bmatrix} = \begin{bmatrix}\boldsymbol{k}_1(\boldsymbol{z}) \\ \boldsymbol{k}_2(\boldsymbol{z})\end{bmatrix} + \begin{bmatrix}A_{11}(\boldsymbol{z}) & A_{12}(\boldsymbol{z}) \\ A_{21}(\boldsymbol{z}) & A_{22}(\boldsymbol{z})\end{bmatrix}\begin{bmatrix}\boldsymbol{z} \\ \boldsymbol{w}\end{bmatrix} + \begin{bmatrix}B_1(\boldsymbol{z}) \\ B_2(\boldsymbol{z})\end{bmatrix}\boldsymbol{u} \tag{12}$$

Here, $\boldsymbol{z}$ represents the controlled output that affects the state equation in a nonlinear fashion. The state vector has been decomposed according to $\boldsymbol{x} = \begin{bmatrix}\boldsymbol{z}^T & \boldsymbol{w}^T\end{bmatrix}^T$, i.e. through a separation between scheduling and non-scheduling states. Accordingly, this class of systems is referred to as 'output-nonlinear' [20]. To arrive at a model of the form Equation 11, consider that the following holds over the equilibrium manifold for every value of $\boldsymbol{z}$ (the subscript $|_{eq}$ to indicate the equilibrium value):

$$\begin{bmatrix}0 \\ 0\end{bmatrix} = \begin{bmatrix}\boldsymbol{k}_1(\boldsymbol{z}) \\ \boldsymbol{k}_2(\boldsymbol{z})\end{bmatrix} + \begin{bmatrix}A_{11}(\boldsymbol{z}) & A_{12}(\boldsymbol{z}) \\ A_{21}(\boldsymbol{z}) & A_{22}(\boldsymbol{z})\end{bmatrix}\begin{bmatrix}\boldsymbol{z} \\ \boldsymbol{w}_{eq}(\boldsymbol{z})\end{bmatrix} + \begin{bmatrix}B_1(\boldsymbol{z}) \\ B_2(\boldsymbol{z})\end{bmatrix}\boldsymbol{u}_{eq}(\boldsymbol{z}) \tag{13}$$

Subtracting Equation 13 from Equation 12 yields:

$$\begin{bmatrix}\dot{\boldsymbol{z}} \\ \dot{\boldsymbol{w}}\end{bmatrix} = \begin{bmatrix}0 & A_{12}(\boldsymbol{z}) \\ 0 & A_{22}(\boldsymbol{z})\end{bmatrix}\underbrace{\begin{bmatrix}\boldsymbol{z} \\ \boldsymbol{w} - \boldsymbol{w}_{eq}(\boldsymbol{z})\end{bmatrix}}_{\triangleq \boldsymbol{w}_{dev}} + \begin{bmatrix}B_1(\boldsymbol{z}) \\ B_2(\boldsymbol{z})\end{bmatrix}\underbrace{\left(\boldsymbol{u} - \boldsymbol{u}_{eq}(\boldsymbol{z})\right)}_{\triangleq \boldsymbol{u}_{dev}} \tag{14}$$

The change of variables in the system state can be completed by considering that $\dot{\boldsymbol{w}}_{dev} = \dot{\boldsymbol{w}} - \dot{\boldsymbol{w}}_{eq}(z) = \dot{\boldsymbol{w}} - \frac{\partial \boldsymbol{w}_{eq}}{\partial z}\dot{z}$. Then, it follows from Equation 14 that

$$\begin{bmatrix} \dot{z} \\ \dot{\boldsymbol{w}}_{dev} \end{bmatrix} = \begin{bmatrix} 0 & A_{12}(z) \\ 0 & A_{22}(z) - \frac{\partial \boldsymbol{w}_{eq}}{\partial z} A_{12}(z) \end{bmatrix} \begin{bmatrix} z \\ \boldsymbol{w}_{dev} \end{bmatrix} + \begin{bmatrix} B_1(z) \\ B_2(z) - \frac{\partial \boldsymbol{w}_{eq}}{\partial z} B_1(z) \end{bmatrix} \boldsymbol{u}_{dev} \tag{15}$$

The resulting system is referred to as *quasi*-LPV (q-LPV) due to the fact that, although it takes the form of Equation 11, the scheduling parameter z is an endogenous system variable. An attractive property of the resulting formulation is that it forms an *equivalent* representation of the original nonlinear system from Equation 12. In other words, *no approximations* are involved, as, for example, in Jacobean linearization.

Despite this equivalence, an extension of the basic ST approach is required for robust control design and analysis purposes. This is a consequence of the fact that any controller implementation involves the total control input $\boldsymbol{u} = \boldsymbol{u}_{dev} + \boldsymbol{u}_{eq}$, whereas the above formulation only considers deviations with respect to the trim input manifold. Consequently, let Equation 15 be augmented as follows:

$$\begin{bmatrix} \dot{z} \\ \dot{\boldsymbol{w}}_{dev} \\ \dot{\boldsymbol{u}}_{eq} \end{bmatrix} = \begin{bmatrix} 0 & A_{12}(z) & 0 \\ 0 & A_{22}(z) - \frac{\partial \boldsymbol{w}_{eq}(z)}{\partial z} A_{12}(z) & 0 \\ 0 & \frac{\partial \boldsymbol{u}_{eq}(z)}{\partial z} A_{12}(z) & 0 \end{bmatrix} \begin{bmatrix} z \\ \boldsymbol{w}_{dev} \\ \boldsymbol{u}_{eq} \end{bmatrix} + \begin{bmatrix} B_1(z) \\ B_2(z) - \frac{\partial \boldsymbol{w}_{eq}(z)}{\partial z} B_1(z) \\ \frac{\partial \boldsymbol{u}_{eq}(z)}{\partial z} B_1(z) \end{bmatrix} \boldsymbol{u}_{dev} \tag{16}$$

Subsequently, a key concept is to consider the time derivative of $\boldsymbol{u}$ as the new control input [20]:

$$\boldsymbol{u}(t) = \int \boldsymbol{\sigma}(t)\, \mathrm{dt} \tag{17}$$

Then, using the change of system state $\boldsymbol{u}_{dev} = \boldsymbol{u} - \boldsymbol{u}_{eq}$ in Equation 16 results in

$$\begin{bmatrix} \dot{z} \\ \dot{\boldsymbol{w}}_{dev} \\ \dot{\boldsymbol{u}}_{dev} \end{bmatrix} = \begin{bmatrix} 0 & A_{12}(z) & B_1(z) \\ 0 & A_{22}(z) - \frac{\partial w_{eq}(z)}{\partial z} A_{12}(z) & B_2(z) - \frac{\partial w_{eq}(z)}{\partial z} B_1(z) \\ 0 & -\frac{\partial \boldsymbol{u}_{eq}(z)}{\partial z} A_{12}(z) & -\frac{\partial \boldsymbol{u}_{eq}(z)}{\partial z} B_1(z) \end{bmatrix} \begin{bmatrix} z \\ \boldsymbol{w}_{dev} \\ \boldsymbol{u}_{dev} \end{bmatrix} + \begin{bmatrix} 0 \\ 0 \\ I \end{bmatrix} \boldsymbol{\sigma} \tag{18}$$

This approach is referred to as *integrator pre-compensation* *. With this formulation, a transforming controller can be constructed *without* feeding back $\boldsymbol{u}_{eq}$. Instead, the controller is augmented with the integrator associated with pre-compensation and the transformation step is fully achieved through the main controller. This results in distinct robustness benefits, which are further elaborated upon in Section III.B.

III. Quasi-LPV Model Framework for (I)NDI-based Control Design

In this section, the principles behind the q-LPV modeling approach introduced in Section II.B.2 are leveraged for the specific case of (I)NDI-based design. The resulting models serve as a basis for robust q-LPV analysis and design for this type of control systems. In doing so, the synergies between these two methods are explained. To show this, the following assumption is made:

Assumption 1: The system in Eq. 12 admits a continuous, admissible control solution $\boldsymbol{u}_{dev}$ and trim map $\boldsymbol{u}_{eq}(z)$ for all $z \in \mathcal{Z}$.

This condition gives rise to the following theorem, which will be revisited later in this section to establish a *duality* between ST q-LPV and (I)NDI-based control:

Theorem 1: Under Assumption 1, the system in Eq. 12 can be transformed to the q-LPV form in Eq. 18.

Proof: The conclusion follows by deduction. Since $\boldsymbol{u} = \boldsymbol{u}_{dev} + \boldsymbol{u}_{eq}(z)$ exists, its first derivative $\boldsymbol{\sigma} = \dot{\boldsymbol{u}} = \dot{\boldsymbol{u}}_{dev} + \frac{\partial \boldsymbol{u}_{eq}(z)}{\partial z}\dot{z}$ also exists. Given that $\dot{z} = A_{12}\boldsymbol{w}_{dev} + B_1\boldsymbol{u}_{dev}$ under the transformation in Eq. 14, it follows that the dynamics governed by $\dot{\boldsymbol{u}}_{dev} = -\frac{\partial \boldsymbol{u}_{eq}(z)}{\partial z}\left(A_{12}\boldsymbol{w}_{dev} + B_1\boldsymbol{u}_{dev}\right) + \boldsymbol{\sigma}$ exist as well. In combination with the intermediate result from Eq. 15, this completes the proof. □

*This concept has strong analogies with velocity-based gain scheduling [9], which has been used successfully in practice [41].

Control-oriented q-LPV models for (I)NDI-based closed-loop systems are presented for a range of inversion strategies in Subsection III.A. Subsection III.B elaborates on how the ST q-LPV and (I)NDI-based transformation strategies give rise to different robustness mechanisms, despite the duality aspect.

A. Modeling inversion strategy

Quasi-LPV models for a range of inversion strategies will be presented. Purely model-based NDI is considered first, where a distinction is made between the inversion of scheduling or non-scheduling states. This is followed by an extension to inversion error compensation as in hybrid INDI and the incorporation of known singular perturbations that prevent full inversion from taking place. Finally, it is shown how the latter representation can be used to establish model formulations for filtered sensor-based INDI.

1. Baseline: model-based inversion

First, a scenario is considered where the scheduling state z forms the controlled variable (CV). Taking the original nonlinear dynamics from Equation 12 as starting point, the inversion law reads as

$$\boldsymbol{u} = B_1^{-1}(z)\left(\boldsymbol{\nu} - \boldsymbol{k}_1(z) - A_{11}(z)z - A_{12}(z)\boldsymbol{w}\right) \tag{19}$$

Application of this controller to Equation 12 leads to the following closed-loop dynamics of the transformed plant:

$$\begin{bmatrix}\dot{z}\\ \dot{\boldsymbol{w}}\end{bmatrix} = \begin{bmatrix}0\\ \boldsymbol{k}_2(z) - B_2^*(z)\boldsymbol{k}_1(z)\end{bmatrix} + \begin{bmatrix}0 & 0\\ A_{21}(z) - B_2^*(z)A_{11}(z) & A_{22}(z) - B_2^*(z)A_{12}(z)\end{bmatrix}\begin{bmatrix}z\\ \boldsymbol{w}\end{bmatrix} + \begin{bmatrix}I\\ B_2^*(z)\end{bmatrix}\boldsymbol{\nu} \tag{20}$$

$$\triangleq \begin{bmatrix}0\\ \boldsymbol{k}_2^*(z)\end{bmatrix} + \begin{bmatrix}0 & 0\\ A_{21}^*(z) & A_{22}^*(z)\end{bmatrix}\begin{bmatrix}z\\ \boldsymbol{w}\end{bmatrix} + \begin{bmatrix}I\\ B_2^*(z)\end{bmatrix}\boldsymbol{\nu} \tag{21}$$

where $B_2^*(z) \triangleq B_2(z)B_1^{-1}(z)$. As mentioned in Section II.A, assessment of the global asymptotic stability with respect to the origin presumes that the origin is an equilibrium point. This requires the additive nonlinearity $\boldsymbol{k}_2^*(z)$ to vanish in the origin. As a result, the zero dynamics take the form of

$$\begin{bmatrix}0\\ \dot{\boldsymbol{w}}\end{bmatrix} = \begin{bmatrix}0 & 0\\ A_{21}^*(0) & A_{22}^*(0)\end{bmatrix}\begin{bmatrix}0\\ \boldsymbol{w}\end{bmatrix} \tag{22}$$

Consequently, the zero dynamics are globally asymptotically stable with respect to the origin if $A_{22}^*(0)$ is Hurwitz. However, this assessment does not suffice for the purpose of robust control design and analysis, which generally concerns all z over the system's operating domain. Therefore, global asymptotic stability with respect to the complete trim manifold must be considered instead:

$$\begin{bmatrix}0\\ 0\end{bmatrix} = \begin{bmatrix}0\\ \boldsymbol{k}_2^*(z)\end{bmatrix} + \begin{bmatrix}0 & 0\\ A_{21}^*(z) & A_{22}^*(z)\end{bmatrix}\begin{bmatrix}z\\ \boldsymbol{w}_{eq}(z)\end{bmatrix} \tag{23}$$

In accordance with the steps of Eq. 12-15 in Section II.B.2, this results in the following transformed system:

$$\begin{bmatrix}\dot{z}\\ \dot{\boldsymbol{w}}_{dev}\end{bmatrix} = \begin{bmatrix}0 & 0\\ 0 & A_{22}^*(z)\end{bmatrix}\begin{bmatrix}z\\ \boldsymbol{w}_{dev}\end{bmatrix} + \begin{bmatrix}I\\ B_2^*(z) - \frac{\partial \boldsymbol{w}_{eq}(z)}{\partial z}\end{bmatrix}\boldsymbol{\nu} \tag{24}$$

Consequently, global asymptotic stability can be verified for all trajectories $z \in \mathcal{Z}$. For the assessment of robustness, the transformed system is augmented in a similar fashion as in Equation 16:

$$\begin{bmatrix}\dot{z}\\ \dot{\boldsymbol{w}}_{dev}\\ \dot{\boldsymbol{u}}_{eq}\end{bmatrix} = \begin{bmatrix}0 & 0 & 0\\ 0 & A_{22}^*(z) & 0\\ 0 & 0 & 0\end{bmatrix}\begin{bmatrix}z\\ \boldsymbol{w}_{dev}\\ \boldsymbol{u}_{eq}\end{bmatrix} + \begin{bmatrix}I\\ B_2^*(z) - \frac{\partial \boldsymbol{w}_{eq}(z)}{\partial z}\\ \frac{\partial \boldsymbol{u}_{eq}(z)}{\partial z}\end{bmatrix}\boldsymbol{\nu} \tag{25}$$

Finally, the corresponding output equation reads as

$$\boldsymbol{u} = \underbrace{B_1^{-1}(z)\left(\boldsymbol{\nu} - A_{12}(z)\boldsymbol{w}_{dev}\right)}_{\boldsymbol{u}_{dev}} + \boldsymbol{u}_{eq} \tag{26}$$

This formulation bears direct equivalence with Equation 19. This can be verified by substituting the equilibrium input manifold, which is given by

$$\boldsymbol{u}_{eq}(z) = -B_1^{-1}(z)\left(\boldsymbol{k}_1(z) + A_{11}(z)z + A_{12}(z)\boldsymbol{w}_{eq}(z)\right) \tag{27}$$

Second, inversion of the non-scheduling state $\boldsymbol{w}$ is considered. Here, the decomposition $\boldsymbol{w} = \begin{bmatrix}\boldsymbol{w}_\rho{}^T & \boldsymbol{w}_\varsigma{}^T\end{bmatrix}^T$ is used to isolate the controlled variable $\boldsymbol{y}_{CV} = \boldsymbol{w}_\rho$. This results in the following realization of Equation 12:

$$\begin{bmatrix}\dot{z}\\ \dot{\boldsymbol{w}}_\rho\\ \dot{\boldsymbol{w}}_\varsigma\end{bmatrix} = \begin{bmatrix}\boldsymbol{k}_1(z)\\ \boldsymbol{k}_2(z)\\ \boldsymbol{k}_3(z)\end{bmatrix} + \begin{bmatrix}A_{11}(z) & A_{12}(z) & A_{13}(z)\\ A_{21}(z) & A_{22}(z) & A_{23}(z)\\ A_{31}(z) & A_{32}(z) & A_{33}(z)\end{bmatrix}\begin{bmatrix}z\\ \boldsymbol{w}_\rho\\ \boldsymbol{w}_\varsigma\end{bmatrix} + \begin{bmatrix}B_1(z)\\ B_2(z)\\ B_3(z)\end{bmatrix}\boldsymbol{u} \tag{28}$$

From here on, the procedure is very similar as before. For clarity, the inversion law reads as:

$$\boldsymbol{u} = B_2^{-1}(z)\left(\boldsymbol{\nu} - \boldsymbol{k}_2(z) - A_{12}(z)z - A_{22}(z)\boldsymbol{w}_\rho - A_{22}(z)\boldsymbol{w}_\varsigma\right) \tag{29}$$

Denoting $A^*_{ij}(z) \triangleq A_{ij}(z) - B^*_i(z)A_{2j}(z)$ and $B^*_i(z) \triangleq B_i(z)B_2^{-1}(z)$, the q-LPV formulation takes the form of:

$$\begin{bmatrix}\dot{z}\\ \dot{\boldsymbol{w}}_{\rho,dev}\\ \dot{\boldsymbol{w}}_{\varsigma,dev}\\ \dot{\boldsymbol{u}}_{eq}\end{bmatrix} = \begin{bmatrix}0 & A^*_{12}(z) & A^*_{13}(z) & 0\\ 0 & -\frac{\partial \boldsymbol{w}_{\rho,eq}(z)}{\partial z}A^*_{12}(z) & -\frac{\partial \boldsymbol{w}_{\rho,eq}(z)}{\partial z}A^*_{13}(z) & 0\\ 0 & A^*_{32}(z) - \frac{\partial \boldsymbol{w}_{\varsigma,eq}(z)}{\partial z}A^*_{12}(z) & A^*_{33}(z) - \frac{\partial \boldsymbol{w}_{\varsigma,eq}(z)}{\partial z}A^*_{13}(z) & 0\\ 0 & \frac{\partial \boldsymbol{u}_{eq}(z)}{\partial z}A^*_{12}(z) & \frac{\partial \boldsymbol{u}_{eq}(z)}{\partial z}A^*_{13}(z) & 0\end{bmatrix}\begin{bmatrix}z\\ \boldsymbol{w}_{\rho,dev}\\ \boldsymbol{w}_{\varsigma,dev}\\ \boldsymbol{u}_{eq}\end{bmatrix} + \begin{bmatrix}B^*_1(z)\\ I - \frac{\partial \boldsymbol{w}_{eq}(z)}{\partial z}B^*_1(z)\\ B^*_3(z) - \frac{\partial \boldsymbol{w}_{\varsigma,eq}(z)}{\partial z}B^*_1(z)\\ \frac{\partial \boldsymbol{u}_{eq}(z)}{\partial z}B^*_1(z)\end{bmatrix}\boldsymbol{\nu} \tag{30}$$

with the performance output given as:

$$\boldsymbol{u} = \underbrace{B_2^{-1}(z)(\boldsymbol{\nu} - A_{22}(z)\boldsymbol{w}_{\rho,dev} - A_{23}(z)\boldsymbol{w}_{\varsigma,dev})}_{\boldsymbol{u}_{dev}} + \boldsymbol{u}_{eq} \tag{31}$$

Corollary 1: If there exists a model-based NDI controller for the output-nonlinear system in Eq. 12, then a pre-compensated q-LPV representation as in Eq. 18 also exists.

Proof: Since Eq. 26 and 31 show that an NDI controller of this type can always be expressed as $\boldsymbol{u} = \boldsymbol{u}_{dev} + \boldsymbol{u}_{eq}$, the proof of Corollary 1 follows immediately from Theorem 1. □

2. Incorporating inversion error compensation

For reasons of brevity, only the special scenario where $\boldsymbol{y}_{CV} = \boldsymbol{w}$ is considered in the sequel[†]. This can be naturally extended to the more general cases from the preceding section based on the insights presented there. Still, this scenario is typical for aerospace systems, where it is common to invert, e.g., low-level dynamics that are nonlinear functions of the aerodynamic variables.

To incorporate the effect of inversion error compensation as in hybrid INDI, the CV dynamics are extended with an additive disturbance term as follows:

$$\underbrace{\dot{\boldsymbol{w}}}_{\triangleq\, \dot{\boldsymbol{y}}^{(SB)}} = \underbrace{\boldsymbol{k}_2(z) + A_{21}(z)z + A_{22}(z)\boldsymbol{w} + B_2(z)\boldsymbol{u}}_{\triangleq\, \dot{\boldsymbol{y}}^{(MB)}} + B_2(z)\boldsymbol{d}_i \tag{32}$$

This shows that sensor-based predictions result in direct observation of the input disturbance signal. Consequently, this leads to the following inversion error compensation equation:

$$\dot{\boldsymbol{y}}^{(HB)} = (I - K_c(z)H_c)\dot{\boldsymbol{y}}^{(MB)} + K_c(z)H_c\dot{\boldsymbol{y}}^{(SB)} = \dot{\boldsymbol{y}}^{(MB)} + K_c(z)H_cB_2(z)\boldsymbol{d}_i \triangleq \dot{\boldsymbol{y}}^{(MB)} + K_c(z)\tilde{\boldsymbol{e}}_\xi \tag{33}$$

It is recalled here that K_c and H_c represent the compensation gain and filter elements, respectively. In light of gain scheduling, both can be configured as nonlinear functions of z, as reflected in the above equation. The compensation

[†]The material in this section draws further on the work in [39].

filter introduces additional states, which must be incorporated in the q-LPV representation. To this end, the following canonical realization is considered in light of Equation 33:

$$H_c : \begin{cases} \dot{\tilde{\boldsymbol{e}}}_\xi = -A_c(z)\tilde{\boldsymbol{e}}_\xi + B_c(z)B_2(z)\boldsymbol{d}_i \\ \boldsymbol{u}_c = \tilde{\boldsymbol{e}}_\xi \end{cases} \tag{34}$$

Working out the derivation along similar lines as before leads to the following control-oriented q-LPV model:

$$\begin{bmatrix} \dot{\boldsymbol{z}} \\ \dot{\boldsymbol{w}}_{dev} \\ \dot{\boldsymbol{u}}_{eq} \\ \dot{\tilde{\boldsymbol{e}}}_\xi \end{bmatrix} = \begin{bmatrix} 0 & A^*_{12}(z) & 0 & -B^*_1(z)K_c(z) \\ 0 & -\frac{\partial \boldsymbol{w}_{eq}(z)}{\partial z}A^*_{12}(z) & 0 & -\left(I - \frac{\partial \boldsymbol{w}_{eq}(z)}{\partial z}B^*_1(z)\right)K_c(z) \\ 0 & \frac{\partial \boldsymbol{u}_{eq}(z)}{\partial z}A^*_{12}(z)) & 0 & 0 \\ 0 & 0 & 0 & -A_c(z) \end{bmatrix} \begin{bmatrix} \boldsymbol{z} \\ \boldsymbol{w}_{dev} \\ \boldsymbol{u}_{eq} \\ \tilde{\boldsymbol{e}}_\xi \end{bmatrix} + \begin{bmatrix} B^*_1(z) \\ I - \frac{\partial \boldsymbol{w}_{eq}(z)}{\partial z}B^*_1(z) \\ \frac{\partial \boldsymbol{u}_{eq}(z)}{\partial z}B^*_1(z) \\ 0 \end{bmatrix} \boldsymbol{\nu} + \begin{bmatrix} 0 \\ B_2(z) \\ 0 \\ B_c(z)B_2(z) \end{bmatrix} \boldsymbol{d}_i \tag{35}$$

with the performance output resulting as:

$$\boldsymbol{u} = \underbrace{B_2^{-1}(z)(\boldsymbol{\nu} - A_{22}(z)\boldsymbol{w}_{dev} - K_c(z)\tilde{\boldsymbol{e}}_\xi)}_{\boldsymbol{u}_{dev}} + \boldsymbol{u}_{eq} \tag{36}$$

The disturbance feedthrough directly reflects the robustness implications of the hybrid inversion loop. The compensation parameters (K_c and H_c) determine how this term gets attenuated through the inversion loop.

Corollary 2: If there exists a hybrid INDI controller for the output-nonlinear system in Eq. 12, then a pre-compensated q-LPV representation as in Eq. 18 also exists.

Proof: The proof of Corollary 2 is analogous to Corollary 1. □

3. Incorporating singular perturbations

In the discussion so far, it has been implicitly assumed that exact inversion of the controlled variable is feasible. However, this is fundamentally not the case for real systems, which are affected by additional singular perturbations due to the presence of e.g., actuators, filters, unsteady aerodynamics, and higher-order structural dynamics. Therefore, inversion *distortions* are a fundamental reality [29]. Where known, these effects should be taken into account in the q-LPV model representation. To this end, an *approximate* inversion law with filtered input is considered:

$$\boldsymbol{u} = B_2^{-1}(z)\boldsymbol{\nu} + \boldsymbol{\phi} \tag{37}$$

The variable $\boldsymbol{\phi}$ refers to the exact inversion input signal affected by a singular perturbation. For the purpose of brevity, this perturbation is considered to be of first order here. However, as demonstrated later in Section V, the insights obtained apply to more general cases as well. For hybrid INDI, this scenario amounts to:

$$\begin{aligned} \epsilon\dot{\boldsymbol{\phi}} &= -\boldsymbol{\phi} - B_2^{-1}(z)\left[\boldsymbol{k}_2(z) + A_{21}(z)\boldsymbol{z} + A_{22}(z)\boldsymbol{w} + K_c(z)\tilde{\boldsymbol{e}}_\xi\right] \\ &= -\boldsymbol{\phi} - B_2^{-1}(z)\left[A_{22}(z)\boldsymbol{w}_{dev} + K_c(z)\tilde{\boldsymbol{e}}_\xi\right] + \boldsymbol{u}_{eq}(z) \end{aligned} \tag{38}$$

Here, $\epsilon \to 0$ represents a small constant that enables the construction of a singular perturbation model [40]. Setting this variable to zero leads to a fundamental change of the nature of the inverted system, since ideal inversion is recovered in this case. Using this framework, the q-LPV model that describes the singularly perturbed hybrid INDI control system takes the form of:

$$\begin{bmatrix} \dot{\boldsymbol{z}} \\ \dot{\boldsymbol{w}}_{dev} \\ \dot{\boldsymbol{u}}_{eq} \\ \dot{\tilde{\boldsymbol{e}}}_\xi \\ \epsilon\dot{\boldsymbol{\phi}} \end{bmatrix} = \begin{bmatrix} \begin{bmatrix} & A_{st}(z) & \end{bmatrix} & \begin{bmatrix} -B_{st}(z) \end{bmatrix} & 0 & \begin{bmatrix} B_{st}(z) \end{bmatrix} \\ 0 & 0 & 0 & -A_c(z) & 0 \\ 0 & -B_2^{-1}(z)A_{22}(z) & I & -B_2^{-1}(z)K_c(z) & -I \end{bmatrix} \begin{bmatrix} \boldsymbol{z} \\ \boldsymbol{w}_{dev} \\ \boldsymbol{u}_{eq} \\ \tilde{\boldsymbol{e}}_\xi \\ \boldsymbol{\phi} \end{bmatrix} + \begin{bmatrix} \begin{bmatrix} B_\nu(z) \end{bmatrix} \\ 0 \\ 0 \end{bmatrix} \boldsymbol{\nu} + \begin{bmatrix} 0 \\ B_2(z) \\ 0 \\ B_c(z)B_2(z) \\ 0 \end{bmatrix} \boldsymbol{d}_i \tag{39}$$

where Equation 37 represents the performance output. The complete derivation is presented in Appendix A. Comparing this result to Equation 35 shows that there remains a coupling between $\boldsymbol{u}_{eq}$ and the transformed states. This directly reflects the impact of inversion distortion on system stability and performance. With this formulation, the impact of singular perturbations can be analyzed systematically over the system's operating range.

4. Special case: filtered sensor-based form

Finally, a special case of the singular perturbation form is discussed. This concerns filtered sensor-based inversion, which is equivalent to hybrid INDI with $K_c = I$ and the model prediction signal disconnected. In this case, the compensation filter H_c can be considered as a singular perturbation. This leads to the following q-LPV model:

$$\begin{bmatrix} \dot{\boldsymbol{z}} \\ \dot{\boldsymbol{w}}_{dev} \\ \dot{\boldsymbol{u}}_{eq} \\ \epsilon\dot{\boldsymbol{\phi}} \end{bmatrix} = \begin{bmatrix} \begin{bmatrix} A_{st}(z) \\ 0 \quad -B_2^{-1}(z)A_{22}(z) \end{bmatrix} \begin{bmatrix} -B_{st}(z) \\ I \end{bmatrix} \begin{bmatrix} B_{st}(z) \\ -I \end{bmatrix} \end{bmatrix} \begin{bmatrix} \boldsymbol{z} \\ \boldsymbol{w}_{dev} \\ \boldsymbol{u}_{eq} \\ \boldsymbol{\phi} \end{bmatrix} + \begin{bmatrix} \begin{bmatrix} B_\nu(z) \\ 0 \end{bmatrix} \end{bmatrix} \boldsymbol{\nu} + \begin{bmatrix} 0 \\ B_2(z) \\ 0 \\ -I \end{bmatrix} \boldsymbol{d}_i \tag{40}$$

Similar comments can be made as before regarding the impact of inversion distortion. The distortion effect becomes more prominent as ϵ takes larger values, i.e., when the filter bandwidth is reduced. This relates to the concept of time-scale separation [34] that is commonly referred to in sensor-based INDI derivations.

Corollary 3: If there exists a sensor-based INDI controller for the output-nonlinear system in Eq. 12, then a pre-compensated q-LPV representation as in Eq. 18 also exists.

Proof: The proof draws from Appendix A. Using the change of variables $\boldsymbol{\phi} = \boldsymbol{\psi} + \boldsymbol{u}_{eq}(z)$, the sensor-based INDI control law can be expressed as $\boldsymbol{u} = B_2^{-1}(z)\boldsymbol{\nu} + \boldsymbol{\psi} + \boldsymbol{u}_{eq} \triangleq \boldsymbol{u}_{dev} + \boldsymbol{u}_{eq}$. Consequently, the conclusion follows along the same lines as Corollaries 1 and 2. □

B. Duality and robustness

Based on Theorem 1 and Corollaries 1-3, (I)NDI-based controllers can be viewed as structured counterparts of direct q-LPV control. This *duality* is underscored by restating Equation 17 for the specific case of (I)NDI-based control:

$$\boldsymbol{u}_{dev}^{(I)NDI}(t) + \boldsymbol{u}_{eq}(t) \mapsto \int \boldsymbol{\sigma}(t)\, \mathrm{dt} \tag{41}$$

Consequently, (I)NDI effectively imposes a particular mapping on the signal $\boldsymbol{\sigma}$. This is in contrast to direct ST q-LPV control, which provides the opportunity for mapping $\boldsymbol{\sigma}$ through *alternative* control schemes. As a result, a fundamentally different transformation structure can be established:

- With (I)NDI-based control, plant transformation forms an explicit part of the controller structure. This concerns the inner inversion loop, which leads to the cancellation of nonlinearities and directly incorporates $\boldsymbol{u}_{eq}$. Consequently, explicit information about the inner loop is required for robust analysis and synthesis.
- Direct q-LPV control based on integrator pre-compensation provides the flexibility to *eliminate* the inner loop signal $\boldsymbol{u}_{eq}$ altogether. As a result, no inner feedback loop is required and the plant transformation step is resolved *implicitly* through integrator pre-compensation and a (generally unstructured) outer loop controller.

Due to its feedback nature, the type of transformation directly affects robustness. Figure 1 serves to illustrate this aspect. Here, the ST q-LPV and (I)NDI-based transformation interconnections are visualized in a single (combined)

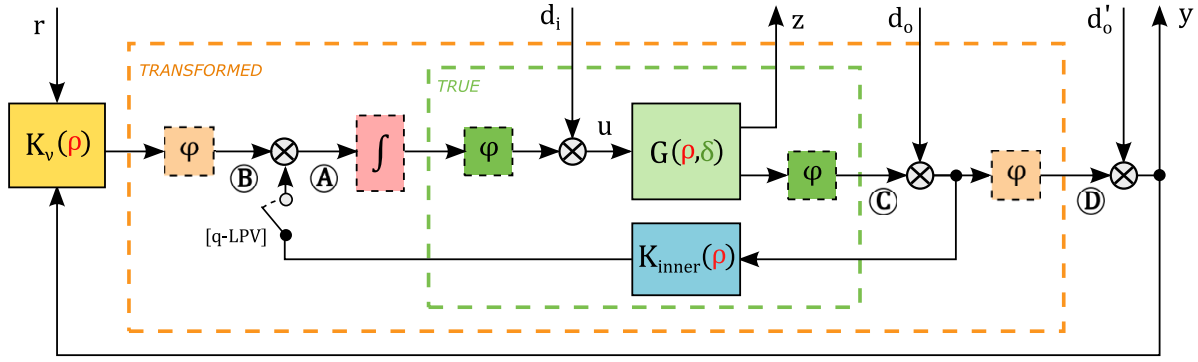

Fig. 1 Generalized plant transformation interconnection; both direct q-LPV and INDI setups are shown, where the former is obtained by switching off the inner feedback loop and adding integral action at the true plant input.

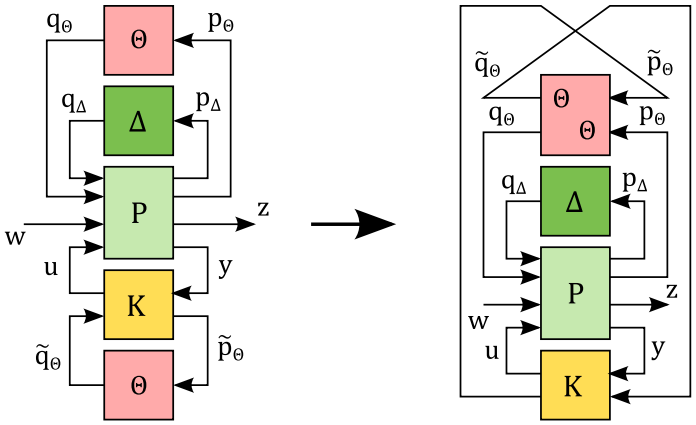

Fig. 2 LFT interconnection of LPV control structure (adapted from [16]).

diagram. Of central importance in the figure are the perturbations (uncertainties) ϕ, which form the basis for robust analysis and design. These are shown at various locations in the feedback loop at the level of the physical ("true") plant and its transformed ("virtual") counterpart. Considering input locations A and B, it becomes apparent that the interaction between the inner transformation signal $\boldsymbol{u}_{eq}$ and the respective perturbations is of fundamentally different nature. This implies that the robustness margins found for the transformed system (loc. B) are strictly not indicative of robustness at the level of the true plant (loc. A). This similarly applies to robustness at the output (loc. C and D). This is of critical importance, as only those perturbations that arise at the true plant are relevant to robust analysis and design. By eliminating the inner feedback loop, the robustness implications induced by $\boldsymbol{u}_{eq}$ are mitigated. As discussed in [20], this is the rationale behind the pre-compensated q-LPV control approach outlined in Section II.B.2. For (I)NDI-based design, key robustness implications of $\boldsymbol{u}_{eq}$ can be accounted for using the q-LPV models derived in this section.

IV. $\mathcal{H}_\infty$-Synthesis of Structured q-LPV Controllers

With the synergies and fundamental differences between q-LPV and (I)NDI-based control being identified, it is of interest to investigate how these approaches compare quantitatively in a robust q-LPV design context. In broad terms, LPV control design can be categorized into three approaches: polytopic [11], LFT [16, 42], and grid-based [17].

Polytopic LPV synthesis requires an affine dependence of the scheduling parameters, which span a polytopic region that is described by a convex hull of a finite set of vertices. This approach yields strong stability and performance guarantees, but may also result in (overly) pessimistic results due to the affine model limitation. The LFT approach can be considered more general in this sense, as it allows the state-space matrices to feature a rational dependency on the scheduling parameters. However, conservativeness is also a known issue for LFT-based synthesis [6]. This is due to the fact that the scheduling parameter rate-of-change is considered to be unbounded when quadratic stability analysis is performed. Grid-based synthesis can be used to address this, as it allows for the explicit incorporation of rate bounds. However, the fact that synthesis is limited to a finite grid of scheduling parameters implies that no guarantees are obtained in-between operating points. Therefore, grid selection becomes an important aspect of the synthesis process, and additional a-posteriori analysis may be required.

In the remainder of this paper, the focus will be on LPV synthesis of structured controllers (such as INDI) using the LFT approach. This enables a synthesis strategy based on non-smooth $\mathcal{H}_\infty$-synthesis techniques. The corresponding structured LFT synthesis formulation and synthesis routine are presented in this section.

A. LFT synthesis formulation

The principles of LFT-based LPV control are briefly reviewed first[‡]. In general, LPV control structures with linear fractional dependence on the scheduling parameter can be considered as shown on the left of Figure 2. The operator T that represents the closed-loop mapping between exogenous inputs $\boldsymbol{w}$ and outputs $\boldsymbol{z}$ takes the form of

[‡]For the full technical details, the authors refer to [16, 42].

$$T(P, K, \Theta) = \mathcal{F}_l \left[\mathcal{F}_u \left(\Theta, P \right), \mathcal{F}_l \left(K, \Theta \right) \right] \tag{42}$$

Here, $\mathcal{F}_l$ and $\mathcal{F}_u$ represent the lower and upper linear fractional transformation, respectively. The parameter block has a block-diagonal structure according to $\Theta = \text{blockdiag}(\rho_1 I_{r1}, \ldots, \rho_k I_{rk})$. With slight abuse of notation, the performance level is described by the induced $\mathcal{L}_2$-gain according to [16]:

$$\max_{\|\Theta\|_\infty \leq 1/\gamma} \|T(P, K, \Theta)\|_\infty < \gamma \tag{43}$$

A distinct characteristic of the LPV control structure is that the scheduling parameter associated with the open-loop plant directly enters the control law as well. Consequently, the LFT interconnection can be reorganized as shown on the right-hand side of Figure 2. This shows that the combined perturbation block has a repeated block-diagonal structure. The resulting operator T can be rewritten as:

$$T(P, K, \Theta) = \mathcal{F}_u \left(\mathcal{F}_l \left(P_a, K \right), \begin{bmatrix} \Theta & 0 \\ 0 & \Theta \end{bmatrix} \right) \tag{44}$$

where the general plant P_a is augmented with additional control channels. Consequently, the transformed LPV control problem takes a form similar to that found in μ-analysis problems [43]. This enables $\mathcal{H}_\infty$-synthesis of parameter-dependent controllers based on an augmented LTI formulation. The nonlinear and time-varying nature of the structured perturbation block is accounted for by adopting static, full-block similarity scalings according to [16]:

$$L_{\Theta \oplus \Theta} \triangleq \left\{ \begin{bmatrix} L_1 & L_2 \\ L_2^T & L_3 \end{bmatrix} > 0 : \quad L_1, L_3 \in L_\Theta \quad \text{and} \quad L_2 \Theta = \Theta L_2 \quad \forall \Theta \in \boldsymbol{\Theta} \right\} \tag{45}$$

where

$$L_\Theta \triangleq \{ L > 0 : \quad L\Theta = \Theta L, \quad \forall \Theta \in \boldsymbol{\Theta} \} \subset \mathcal{R}^{r \times r} \tag{46}$$

Application of the small-gain theorem [44] results in a translation of the robust performance condition from Equation 43 to the following scaled $\mathcal{H}_\infty$ formulation for gain-scheduled controllers [16]:

$$\left\| \begin{bmatrix} L^{1/2} & \\ & I \end{bmatrix} \mathcal{F}_l \left(P_a, K \right) \begin{bmatrix} L^{-1/2} & \\ & I \end{bmatrix} \right\|_\infty < \gamma \tag{47}$$

Consequently, the synthesis problem is to find similarity scalings L and structure control K such that γ is minimized. As presented in [16], the particular structure of the linear-fractional LPV setup leads to solvability conditions that are convex in the full-order case. Iterative techniques like DK-iteration[§] [3, 45] are therefore not required for this class of problems, as synthesis can be performed directly based on a system of Linear Matrix Inequalities (LMIs). However, this generally does not apply to controllers that are of fixed, low-order structure. This scenario is discussed next.

B. Non-smooth synthesis

For control structures $K(\boldsymbol{\kappa})$ that are parametrized by design parameters $\boldsymbol{\kappa} \in \mathcal{K}$, the synthesis objective based on Equation 47 takes the form of

$$\min_{\boldsymbol{\kappa} \in \mathcal{K}, L \in L_{\Theta \oplus \Theta}} \gamma \quad \text{such that} \quad \left\| \begin{bmatrix} L^{1/2} & \\ & I \end{bmatrix} \mathcal{F}_l \left(P_a, K(\boldsymbol{\kappa}) \right) \begin{bmatrix} L^{-1/2} & \\ & I \end{bmatrix} \right\|_\infty < \gamma \tag{48}$$

The decision variables $\boldsymbol{\kappa}$ can be optimized using a non-smooth $\mathcal{H}_\infty$-synthesis algorithm [46] with explicit constraints on the positive realness of the similarity scaling L and its elements, as reflected by Equations 45-46. This can be achieved using, for example, MATLAB® `systune` [47, 48]. The design parameter and scaling matrix can be optimized simultaneously, i.e., without separate iterations between synthesis and analysis steps. Moreover, the scaling constraint from Equation 45 can be incorporated as a passivity constraint with appropriate structure between the input and output channels of the corresponding multiplier block:

$$\int_0^T \boldsymbol{q}_L(t)^T \boldsymbol{p}_L(t) \mathrm{d}t > 0 \tag{49}$$

which enforces L to be strict positive real. Similar considerations apply to the constraint from Equation 46.

[§]This procedure alternates between the controller (K) synthesis and scaling (D) optimization steps until convergence.

V. Case Study

In the sequel, it is shown how the techniques presented in the preceding sections can be leveraged to synthesize INDI-based controllers for a nonlinear aeroservoelastic wing section simulation model. The resulting INDI-based control designs are subsequently compared with direct q-LPV control. This sheds light on the robustness implications of the INDI transformation structure.

A. Aeroservoelastic wing section model

The aeroservoelastic simulation model under consideration has been used in previous control design studies using LPV [49], NDI [50], and other methods [51, 52]. The dynamics are modeled as a second-order system in both pitch and plunge directions, governed by quasi-steady aerodynamics. Consequently, the equations of motion take the form of:

$$M \begin{bmatrix} \ddot{h} \\ \ddot{\alpha} \end{bmatrix} = (-K(\alpha) + F_x(V_0)) \begin{bmatrix} h \\ \alpha \end{bmatrix} + (-C + F_{\dot{x}}(V_0)) \begin{bmatrix} \dot{h} \\ \dot{\alpha} \end{bmatrix} + F_u(V_0) \begin{bmatrix} \beta_l \\ \beta_t \end{bmatrix} \tag{50}$$

where the nonlinear stiffness matrix $K(\alpha) = \begin{bmatrix} k_h & 0 \\ 0 & k_\alpha(1+\delta_{k_\alpha}(\alpha)) \end{bmatrix}$ and aerodynamic terms $F_\bullet(V_0)$ feature polynomial dependencies on the scheduling parameters. Two control inputs are considered, where β_l and β_t represent the leading-edge and trailing-edge control surfaces, respectively. The corresponding stiffness polynomial is of order four:

$$\delta_{k_\alpha}(\alpha) = c_1\alpha + c_2\alpha^2 + c_3\alpha^3 + c_4\alpha^4; \tag{51}$$

Considering constant values for the free-stream airspeed V_0, Equation 50 be written as an output-nonlinear system of the form presented in Equation 12. To this end, setting $\boldsymbol{z} = [\, h \;\; \alpha \,]^T$, $\boldsymbol{w} = [\, \dot{h} \;\; \dot{\alpha} \,]^T$, and $\boldsymbol{u} = [\, \beta_l \;\; \beta_t \,]^T$ results in:

$$\begin{bmatrix} \dot{\boldsymbol{z}} \\ \dot{\boldsymbol{w}} \end{bmatrix} = \begin{bmatrix} 0 & I \\ M^{-1}\left(-K(\alpha) + F_x(V_0)\right) & M^{-1}\left(-C + F_{\dot{x}}(V_0)\right) \end{bmatrix} \begin{bmatrix} \boldsymbol{z} \\ \boldsymbol{w} \end{bmatrix} + \begin{bmatrix} 0 \\ M^{-1}F_u(V_0) \end{bmatrix} \boldsymbol{u} \triangleq \begin{bmatrix} 0 & I \\ A_{21}(\boldsymbol{z}) & A_{22} \end{bmatrix} \begin{bmatrix} \boldsymbol{z} \\ \boldsymbol{w} \end{bmatrix} + \begin{bmatrix} 0 \\ B_2 \end{bmatrix} \boldsymbol{u} \tag{52}$$

For a complete description of the simulation model, including a more detailed specification of the related parameters, the reader is referred[¶] to [52]. The resulting system dynamics exhibit strong nonlinearities, as illustrated by the simulation result in Figure 3. The simulation shows the emergence of a limit cycle oscillation as the typical wing section is initialized from a nonzero initial condition. The nonlinear behavior is similarly reflected by the pole zero map and frequency responses in Figure 4. These show that the linearized system dynamics consist of badly damped oscillatory modes, whose natural frequencies are functions of the incidence angle. Moreover, the conjugate pole pair associated with one of these modes crosses the imaginary axis, marking a region of instability.

B. Design objectives

The unsatisfactory open-loop system characteristics motivate the design of a feedback controller whose function is to stabilize the system and improve modal damping throughout the operating domain. It is assumed that the full state

[¶]Note that with respect to the original model, the nonlinear dependency on h has been dropped in the present case study.

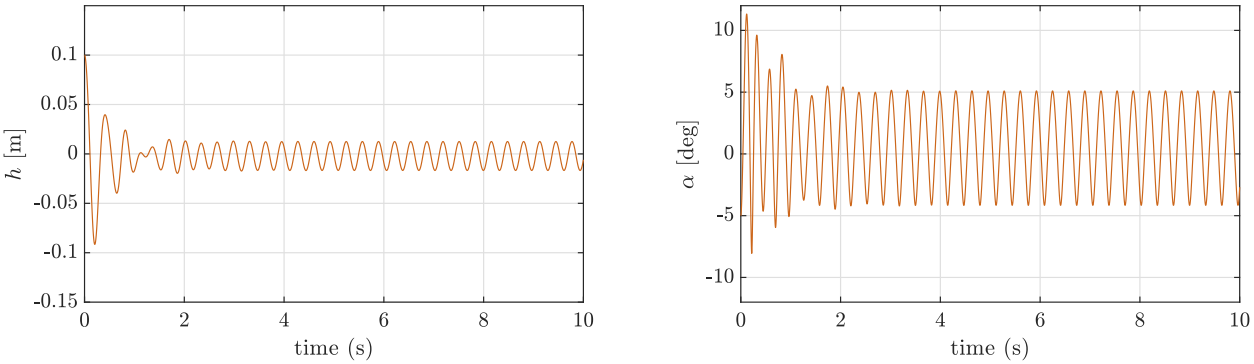

Fig. 3 Nonlinear time-domain simulation to nonzero initial condition (V_0 = 20 m/s).

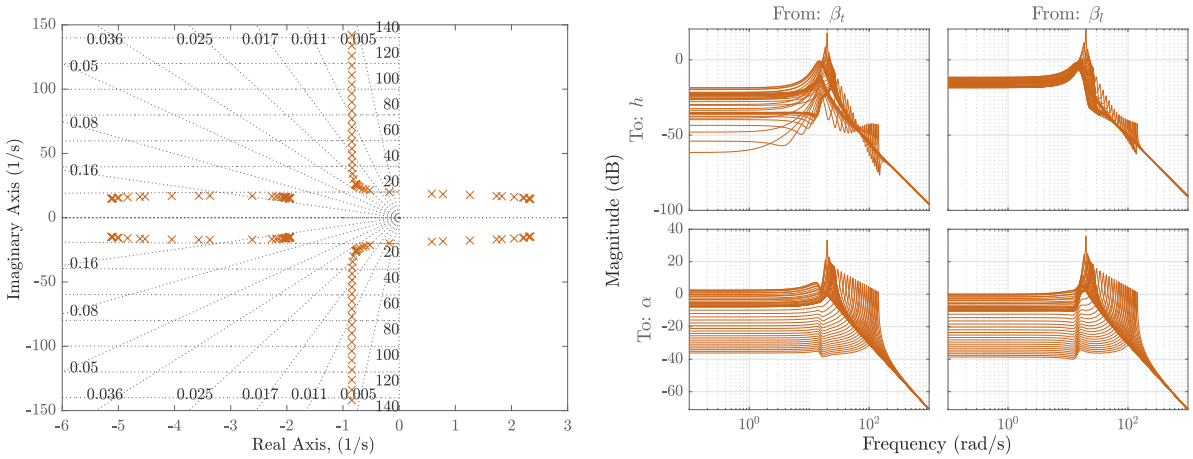

(a) Pole-zero map **(b) Bode diagrams**

Fig. 4 LTI system characteristics as a function of incidence angle $\alpha \in [-10, 10]$ deg. ($V_0 = 20$ m/s).

vector can be measured, which is in line with the state feedback nature of (I)NDI model predictions. In addition to this primary objective, the closed-loop system is subject to auxiliary objectives that relate to robustness and control activity. In particular, the controller should exhibit adequate disk margins in all loops and feature sufficient robustness against high-frequency unmodeled dynamics. Moreover, control activity should be limited to prevent excessive actuator usage. This combination of performance requirements can be accommodated through the following four-block objective:

1) $\boldsymbol{S_oG}$ $\boldsymbol{(\dot{d}_i \rightarrow y)}$ - Suppression of insufficiently damped modes is best achieved through minimization of this objective; moreover, it enables incorporation of additional integral action, whereas the $\mathcal{L}_2$-gain provides an indication of robustness against time-state-dependent parametric perturbations of the form $\boldsymbol{d}_i = \boldsymbol{\delta}(\boldsymbol{x}, t)$;
2) $\boldsymbol{T_i}$ $\boldsymbol{(\dot{d}_i \rightarrow \dot{u})}$ - robustness against high-frequency unmodeled dynamics and noise attenuation on the input channel is achieved by constraining the control bandwidth on this channel;
3) $\boldsymbol{S_o}$ $\boldsymbol{(d_o \rightarrow y)}$ - imposing an upper bound on this objective ensures robustness in terms of S-based disk margins; moreover, in the case of full-state observation where the initial plant state is set as a constant output disturbance $\boldsymbol{d}_o = \boldsymbol{x}_{init}$, its bandwidth can be modulated to achieve a minimum rate of decay of the plant states;
4) $\boldsymbol{KS_o}$ $\boldsymbol{(d_o \rightarrow \dot{u})}$ - represents an indication of control effort due to output disturbances; in line with the above, this relates to control activity due to nonzero initial plant conditions in the full-state observation scenario.

In light of Equation 48, this leads to the following LPV synthesis objective:

$$\min_{\boldsymbol{\kappa}\in\mathcal{K}, L\in L_{\Theta\oplus\Theta}} \gamma \quad \text{such that} \quad \left\| \begin{bmatrix} L^{1/2} & \\ & W_L \end{bmatrix} \begin{bmatrix} T_{q_{\Theta\oplus\Theta}\leftarrow p_{\Theta\oplus\Theta}}(\boldsymbol{\kappa}) & \star & \star \\ \star & T_{S_oG}(\boldsymbol{\kappa}) & T_{S_o}(\boldsymbol{\kappa}) \\ \star & T_{T_i}(\boldsymbol{\kappa}) & T_{KS_o}(\boldsymbol{\kappa}) \end{bmatrix} \begin{bmatrix} L^{-1/2} & \\ & W_R \end{bmatrix} \right\|_\infty < \gamma \tag{53}$$

Table 1 summarizes the selected (constant) weighting function parameters used to minimize the combined upper bound of the four-block system. Note that nominal nonlinear stability is ensured if $L^{1/2} T_{q_{\Theta\oplus\Theta}\leftarrow p_{\Theta\oplus\Theta}} L^{-1/2} < \gamma_{stab} < 1$. In line with Sec. IV.B, Equation 53 is incorporated as a soft design objective in MATLAB® `systune`. This also includes the hard constraint on the scaling L.

Table 1 Robustness and performance weighting functions

Parameter	Value
W_L	$blkdiag(W_{S_oG}, W_{T_i}) = blkdiag(0.126 I_{4\times4}, W_u I_{2\times2})$ with $W_u = 1/600$
W_R	$blkdiag(W_{S_o}, W_{KS_o}) = blkdiag(blkdiag(\frac{1}{2} W_u^{-1} I_{2\times2}, I_{2\times2}), I_{2\times2})$
$W_{dec}(j\omega)$	$\frac{10^{-2} j\omega + 6.28}{j\omega + 6.28(10^{-2})}$

In addition to minimizing the four-block upper bound, a minimum rate of decay of the closed-loop system dynamics is also required. This implies that controller solutions that introduce slow modes must be prevented. In line with the above description, this can be achieved by imposing a minimum bandwidth on the output sensitivity functions associated with h and α at selected operating points:

$$z_{dec}(j\omega) = W_{dec}(j\omega) \begin{bmatrix} S_{o_h,h}(j\omega) & S_{o_h,\alpha}(j\omega) \\ S_{o_\alpha,h}(j\omega) & S_{o_\alpha,\alpha}(j\omega) \end{bmatrix} \begin{bmatrix} d_{o_h}(j\omega) \\ d_{o_\alpha}(j\omega) \end{bmatrix} \tag{54}$$

As shown in Table 1, the filter $W_{dec}(j\omega)$ is configured as a first-order lag-lead. This additional objective is implemented in MATLAB® `systune` as a hard constraint at different operating conditions in a multi-model fashion.

C. Control law structures and synthesis interconnections

To investigate the relative capabilities of INDI-based and direct q-LPV control, three configurations are compared. All designs are based on plant state feedback and feature a total controller order of six states. The first design consists of a hybrid INDI (HB-INDI) loop based on second-order inversion compensation in combination with a non-scheduled, two-state virtual control law K_ν. The displacement h and rotation angle α are selected as the CVs. The rationale behind the use of a second-order scaled complementary filter is to achieve sufficient high-frequency roll-off after differentiation of the CVs. With this structure, nonlinearities are accommodated through the inversion loop only. The second architecture is very similar but has the embedded model disconnected, resulting in a purely sensor-based INDI (SB-INDI) configuration. This design has no gain-scheduled elements and therefore collapses to a pure LTI configuration. Third, a direct q-LPV controller is considered. Two states are reserved for integrator pre-compensation, leaving the outer feedback compensator K to be of order four. The feedback compensator is left unstructured otherwise. Figures 5a and 5b show the block diagrams associated with the INDI and direct q-LPV configurations, respectively.

To synthesize these controllers for the design objectives listed before, the q-LPV modeling insights from Section III are applied to the system at hand. As a starting point, consider the baseline transformed plant as:

$$\begin{bmatrix} \dot{z} \\ \dot{w} \\ \dot{u}_{eq} \end{bmatrix} = \begin{bmatrix} 0 & I & 0 \\ 0 & A_{22} & -B_2 \\ 0 & \frac{\partial u_{eq}(z)}{\partial z} & 0 \end{bmatrix} \begin{bmatrix} z \\ w \\ u_{eq} \end{bmatrix} + \begin{bmatrix} 0 \\ B_2 \\ 0 \end{bmatrix} \underbrace{\left(u_{eq} + u_{dev}\right)}_{=u} \tag{55}$$

Section III shows how this baseline model can be further augmented for INDI-based control. In this light, the decomposition used for the singular perturbation and filtered sensor-based inversion representations from Sections III.A.3-III.A.4 is recalled. This decomposition is used to arrive at a common synthesis framework for the INDI configurations of interest. Substitution of $u = B_2^{-1}\nu + u_{INDI}^{(\bullet)}$ in Equation 55 results in:

$$\begin{bmatrix} \dot{z} \\ \dot{w} \\ \dot{u}_{eq} \end{bmatrix} = \begin{bmatrix} 0 & I & 0 \\ 0 & A_{22} & -B_2 \\ 0 & \frac{\partial u_{eq}(z)}{\partial z} & 0 \end{bmatrix} \begin{bmatrix} z \\ w \\ u_{eq} \end{bmatrix} + \begin{bmatrix} 0 \\ B_2 \\ 0 \end{bmatrix} u_{INDI}^{(\bullet)} + \begin{bmatrix} 0 \\ I \\ 0 \end{bmatrix} \nu + \begin{bmatrix} 0 \\ B_2 \\ 0 \end{bmatrix} d_i \tag{56}$$

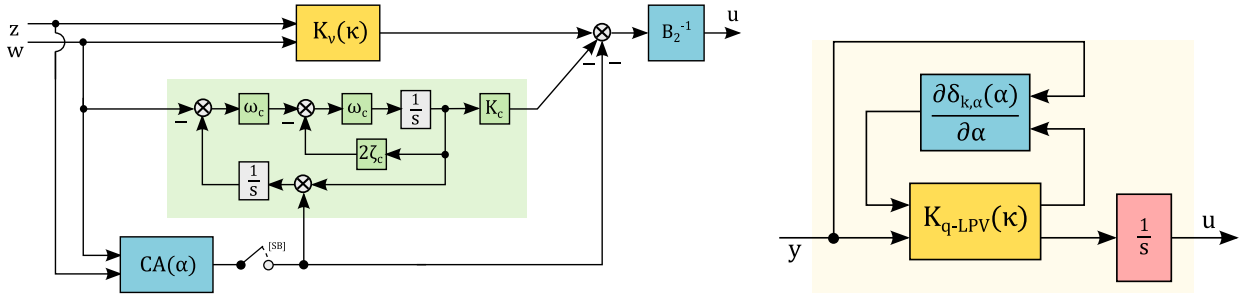

(a) Hybrid/sensor-based INDI controllers **(b) q-LPV controller**

Fig. 5 Controller structures.

For hybrid INDI, the inversion input $\boldsymbol{u}_{INDI}^{(HB)}$ takes the form of:

$$\begin{cases} \dot{\tilde{\boldsymbol{e}}}_{\xi} = -A_c \tilde{\boldsymbol{e}}_{\xi} + B_{c_i} B_2 \boldsymbol{d}_i + B_{c_o} \boldsymbol{d}_o \\ \boldsymbol{u}_{INDI}^{(HB)} = -B_2^{-1} \left(A_{22} \boldsymbol{w} + K_c \tilde{\boldsymbol{e}}_{\xi} \right) + \boldsymbol{u}_{eq} \end{cases} \tag{57}$$

Substitution of this scheme into Equation 56 results in complete cancellation of the nominal dynamics associated with $\dot{\boldsymbol{w}}$. Consequently, full state linearization is achieved in this scenario. Conversely, for sensor-based INDI:

$$\begin{cases} \dot{\boldsymbol{\phi}} = -A_c \boldsymbol{\phi} + B_{c_i} \left(-B_2^{-1} A_{22} \boldsymbol{w} + \boldsymbol{u}_{eq} - \boldsymbol{d}_i \right) - B_{c_o} B_2^{-1} \boldsymbol{d}_o \\ \boldsymbol{u}_{INDI}^{(SB)} = \boldsymbol{\phi} \end{cases} \tag{58}$$

Since the finite filter bandwidth leads to inversion distortions, the resulting nominal dynamics will remain nonlinear. Finally, following Section II.B.2 for the direct q-LPV controller, incorporation of integrator pre-compensation in Equation 55 leads to the following synthesis model:

$$\begin{bmatrix} \dot{z} \\ \dot{\boldsymbol{w}} \\ \dot{\boldsymbol{u}}_{dev} \end{bmatrix} = \begin{bmatrix} 0 & I & 0 \\ 0 & A_{22} & B_2 \\ 0 & -\frac{\partial \boldsymbol{u}_{eq}(z)}{\partial z} & 0 \end{bmatrix} \begin{bmatrix} z \\ \boldsymbol{w} \\ \boldsymbol{u}_{dev} \end{bmatrix} + \begin{bmatrix} 0 \\ 0 \\ I \end{bmatrix} \boldsymbol{\sigma} + \begin{bmatrix} 0 \\ 0 \\ I \end{bmatrix} \dot{\boldsymbol{d}}_i \tag{59}$$

Summarizing, the hybrid and sensor-based INDI designs feature respectively 18 and 17 tunable parameters, compared to 57 parameters for the direct q-LPV controller. Therefore, the latter results in substantially more design degrees of freedom for the same number of states.

The above q-LPV models can be converted to LFT-based LPV representations by expanding the nonlinear term $\frac{\partial \boldsymbol{u}_{eq}(z)}{\partial z}$. From Equation 52 it is found that

$$\frac{\partial \boldsymbol{u}_{eq}(z)}{\partial z} = -B_2^{-1} \frac{\partial A_{21}(z) z}{\partial z} = -F_u^{-1}(V_0) \left(- \begin{bmatrix} k_h & 0 \\ 0 & k_\alpha \left(1 + \frac{\partial \delta_{k_\alpha}(\alpha)\alpha}{\partial \alpha} \right) \end{bmatrix} + F_x(V_0) \right) \tag{60}$$

Consequently, the scheduling parameter is set as:

$$\rho \triangleq \frac{\partial \delta_{k_\alpha}(\alpha)\alpha}{\partial \alpha} = 2c_1\alpha + 3c_2\alpha^2 + 4c_3\alpha^3 + 5c_4\alpha^4 \tag{61}$$

The bounds on the scheduling parameter $\rho \in [a, b]$ directly follow from the operating region $\alpha \in [-10, 10]$ deg. The `LPVTools` MATLAB® toolbox [53] is used to establish the corresponding LFT models. Since the resulting LPV representations are described by a *scalar* $\Theta = \rho$, the similarity scaling L becomes a 2×2 matrix. Figure 6a shows the high-level synthesis interconnection associated with the controller options considered. The INDI configuration results in additional structure at the level of the controller itself, as shown in Figure 6b.

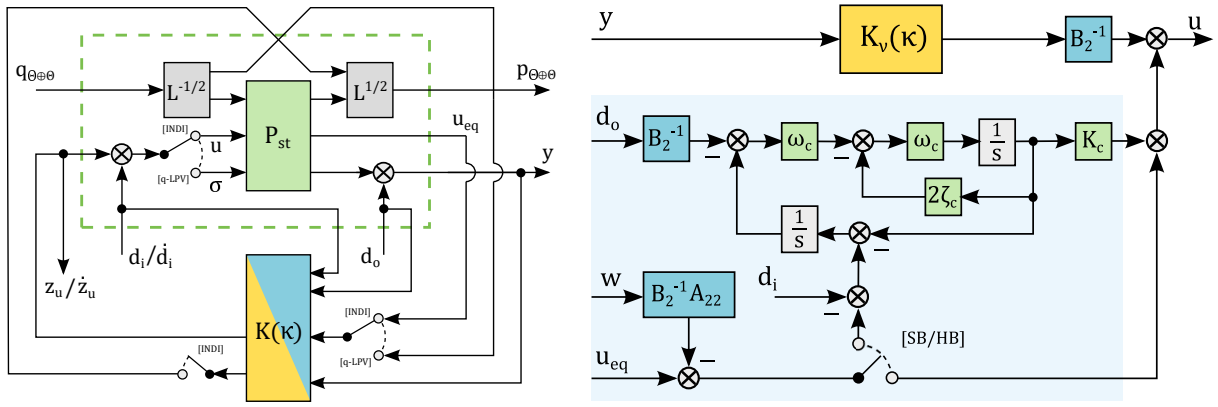

(a) Full synthesis interconnection **(b) INDI synthesis structure**

Fig. 6 Synthesis interconnections.

A few remarks should be made at this point. First, the propagation of the output disturbance signal through the linear parts of the inversion laws has been accounted for. However, for the model prediction term $\boldsymbol{u}_{eq}$ in hybrid INDI, nonlinear propagation of output disturbances cannot be accounted for in the above framework. The robustness analysis in Section V.E will further consider this aspect. Second, in light of the synthesis objectives from Section V.B, the weighting filter imposed on the INDI control input signal must be augmented by additional differentiation according to $z_{\dot{u}}(s) = \frac{s}{\epsilon s+1} z_u(s)$. Consequently, the corresponding input disturbance must be integrated according to $d_i(s) = \frac{1}{s+\epsilon} \dot{d}_i(s)$ for consistency. Here, ϵ is again selected as a small number. Finally, for the same reasons that only stable weighting functions can be used to compute the (bounded) $\mathcal{H}_\infty$-norm, the additional augmentation poles located in the origin of Equation 56 are moved by a small value along the real axis into the left-hand plane.

D. Synthesis results

Using the transformed plant synthesis models, each control law is synthesized using the non-smooth synthesis approach presented in Section IV. Here, the number of random starts performed during the optimization is set to 25. The resulting LPV performance norms are summarized in Table 2. It appears that the q-LPV controller performs best, followed by the hybrid INDI design. The sensor-based INDI controller, being a non-scheduled controller, results in the worst performance levels. Note that for hybrid INDI, the result $\gamma_{stab} = 0$ reflects the fact that full-state linearization is achieved in the nominal case.

To gain further insight into the characteristics of each design, Figures 7 and 8 show the frequency responses associated with each objective over a range of different operating conditions. Similar patterns are observed here. Note that the corresponding LTI models have been obtained in two ways: first, by sampling the q-LPV synthesis models from the previous section for frozen values of the scheduling parameter; and second, through trimming and linearization of the nonlinear closed-loop system based on the implementations shown in Figure 5. Both approaches result in equivalent outcomes, which demonstrates local linear equivalence [7] of the presented q-LPV model formulations. Figure 9 illustrates the closed-loop nonlinear response characteristics associated with each design.

E. Robustness analysis

The frequency responses from Figure 7 exhibit adequate roll-off at high frequencies, which is an indication of robustness against high-frequency unmodeled dynamics. However, the obtained output sensitivity norms are excessively high. The multivariable nature of the output vector leads to a substantial degree of conservativeness here. Therefore, additional analysis is required, which is done by investigating loop-at-a-time disk margins at the plant input and output. Figure 10 shows the corresponding Nichols diagrams.

From these results, it appears that all designs exhibit adequate robustness at the plant input. However, some additional discussion is pertinent for robustness at the plant output. This relates to the missing propagation of $\boldsymbol{d}_o$ through the scheduling block in the synthesis representation, as mentioned in Section V.C. Due to this setup, the synthesis objective effectively relates to location D in Figure 1. Figure 10b shows that good robustness margins are obtained at this location. However, breaking all loops at the sensor location C illustrates a different picture for hybrid INDI. Here, it appears that the additional gain induced by the on-board model leads to substantial degradation of the robustness margins.

Besides additional LTI robustness analysis, further insight into nonlinear robust stability and performance characteristics is also obtained. Figure 11 shows a number of nonlinear simulation results that substantiate to what extent the three controllers tolerate state-dependent input disturbances. Two scenarios are considered. First, an additional alpha-dependency is introduced that is scaled by the constant W_{S_oG} used for synthesis:

$$d_{i_{1,2}} = W_{S_oG}\alpha \tag{62}$$

Table 2 Ordered LPV synthesis norms, incl. decompositions of sub-objectives.

	γ_{syn}	γ_{stab}	γ_{SoG}	γ_{Ti}	γ_{So}	γ_{KSo}
q-LPV	0.98	0.40	0.69	0.83	0.86	0.91
HB-INDI	1.44	0.00	1.01	0.91	0.96	1.41
SB-INDI	2.06	0.53	1.31	1.18	1.80	2.06

Table 3 Optimal INDI tunable inversion parameters returned by synthesis.

	K_c (-)	ω_c (rad/s)
Hybrid	1.00	159
Sensor-based	n/a	197

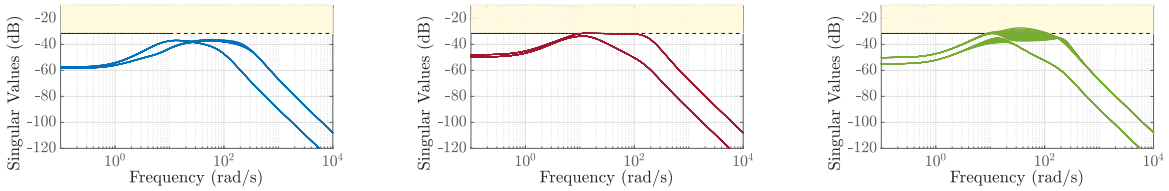

(a) Input disturbance rej. (q-LPV) **(b) Input disturbance rej. (HB-INDI)** **(c) Input disturbance rej. (SB-INDI)**

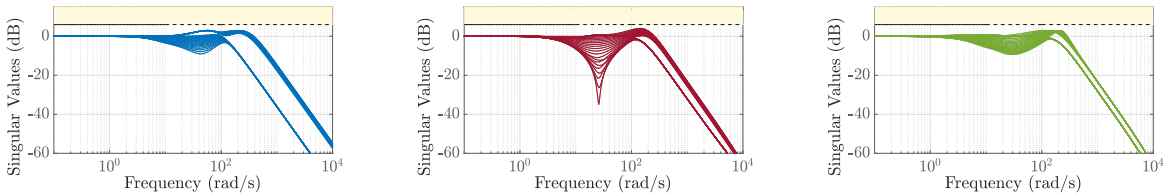

(d) Input compl. sensitiv. (q-LPV) **(e) Input compl. sensitiv. (HB-INDI)** **(f) Input compl. sensitiv. (SB-INDI)**

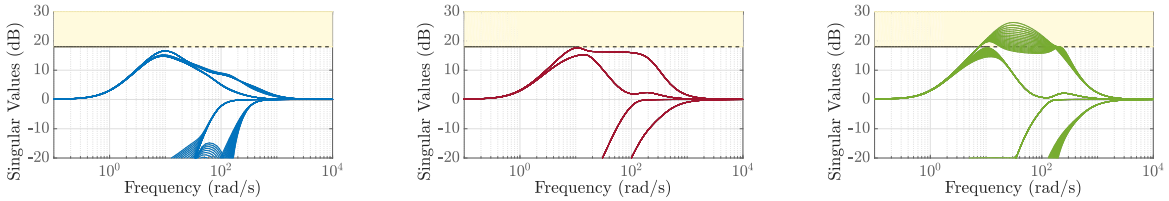

(g) Output Sensitivity (q-LPV) **(h) Output Sensitivity (HB-INDI)** **(i) Output Sensitivity (SB-INDI)**

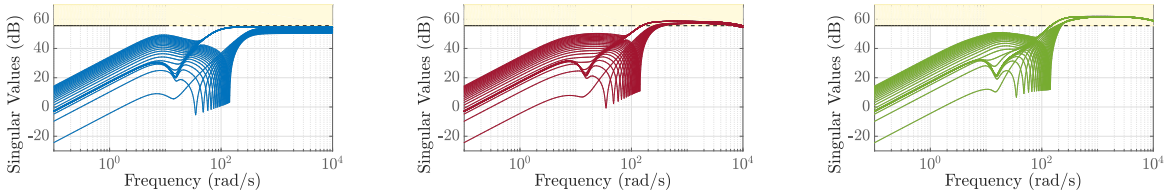

(j) Controller times output sensitivity (q-LPV) **(k) Controller times output sensitivity (HB-INDI)** **(l) Controller times output sensitivity (SB-INDI)**

Fig. 7 Performance objectives over sampled parameter grid.

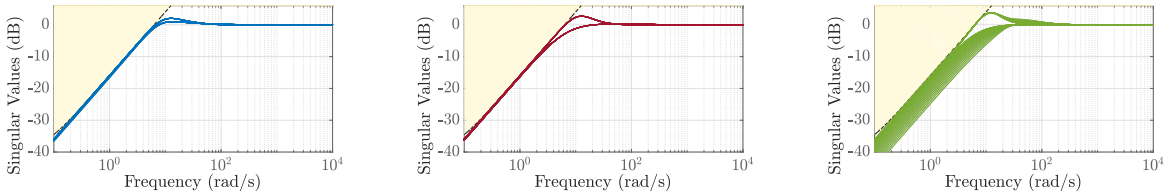

(a) q-LPV **(b) HB-INDI** **(c) SB-INDI**

Fig. 8 Output sensitivity constraint over sampled parameter grid.

With this perturbation, the analysis parallels the insights obtained previously regarding input disturbance rejection performance. The corresponding time-domain histories are shown in Figure 11a. Similar observations apply as before, with direct q-LPV control exhibiting the smallest and sensor-based INDI control the largest discrepancies from nominal performance, respectively.

Second, sampled parametric uncertainty is considered for the nonlinear stiffness polynomial $\delta_{k_\alpha}(\alpha)$. Here, the polynomial offset has been transformed to match the plant input according to:

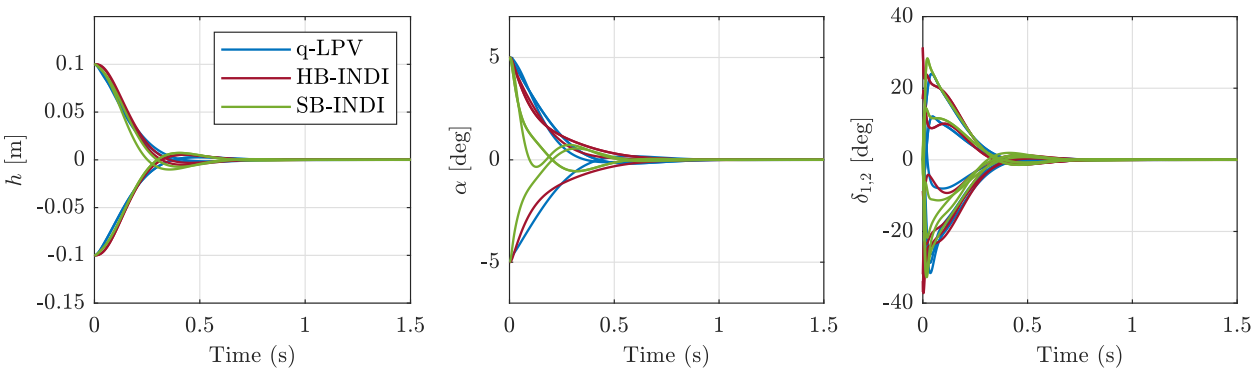

Fig. 9 Closed-loop nonlinear time-domain simulation to nonzero initial condition (V_0 = 20 m/s).

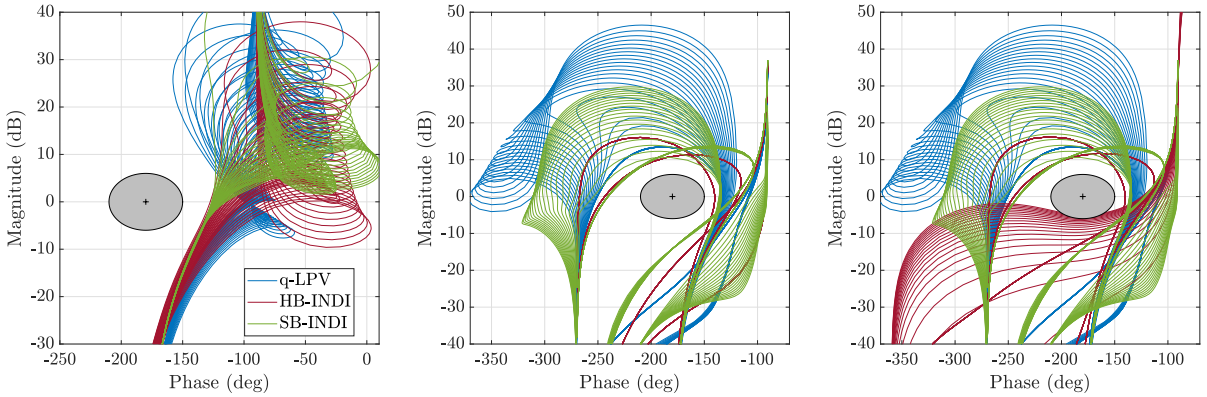

(a) Plant input (loc. A) **(b) Scheduling loop closed (loc. D)** **(c) Plant output (loc. C)**

Fig. 10 Loop-at-a-time Nichols diagrams over sampled parameter grid; for reference, a disk-shaped exclusion zone corresponding to 6dB gain margin and 30° phase margin has been included.

$$\boldsymbol{d}_i = \boldsymbol{w}_{nl}(\alpha) = F_u^{-1}(V_o) \begin{bmatrix} 0 \\ k_\alpha \Delta\delta_{k_\alpha}(\alpha) \end{bmatrix} \alpha \tag{63}$$

The simulation results are shown in Figure 11b. The diagrams shown on the bottom row show how the sampled uncertainty signals compare to the bound corresponding to W_{S_oG}. In most cases, the induced disturbance terms remain well within the baseline sector bounds. However, the hybrid INDI control law results in larger deviations. Worse, there is one instance where the sector bounds are exited and the closed-loop system becomes unstable. This can be attributed to fast transients induced by model offsets, which do not feature any form of bandwidth limitation with respect to KS_o. These transients cause the system to get perturbed further away from its initial condition, causing the nonlinear offset to grow in terms of its absolute norm. Therefore, as shown before in the broken-loop analysis, the use of model predictions introduces additional effects that one must be aware of.

F. Further insights

The case study in this section illustrates several key robustness implications associated with INDI. It is shown how the INDI and q-LPV controller setups can be related to a common basis in terms of their respective q-LPV synthesis models. However, the different control structures that go along with each approach lead to important disparities. As discussed in Section III.B, the structure of the INDI setup is such that $\boldsymbol{u}_{eq}$ effectively enters the control law directly through the inversion loop. Moreover, the inversion loop is the only element through which gain scheduling is performed in the configuration presented here. This is in contrast to the q-LPV controller, which completely eliminates feedback of $\boldsymbol{u}_{eq}$ and exploits more degrees of freedom to achieve gain scheduling to maximize performance and robustness for the

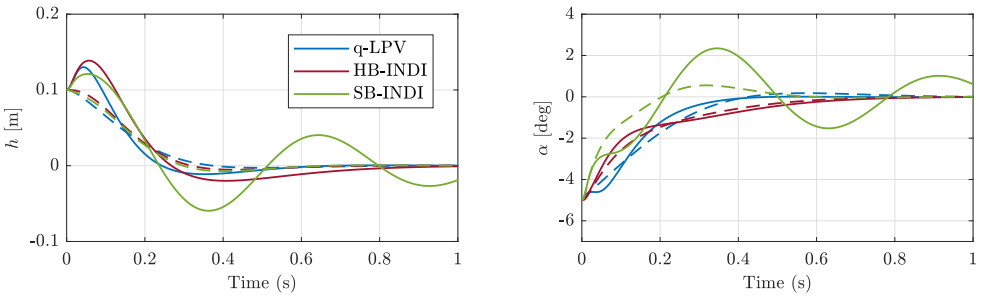

(a) Alpha-dependent input disturbance weighted by W_{SoG}; the nominal response is indicated using dashed lines.

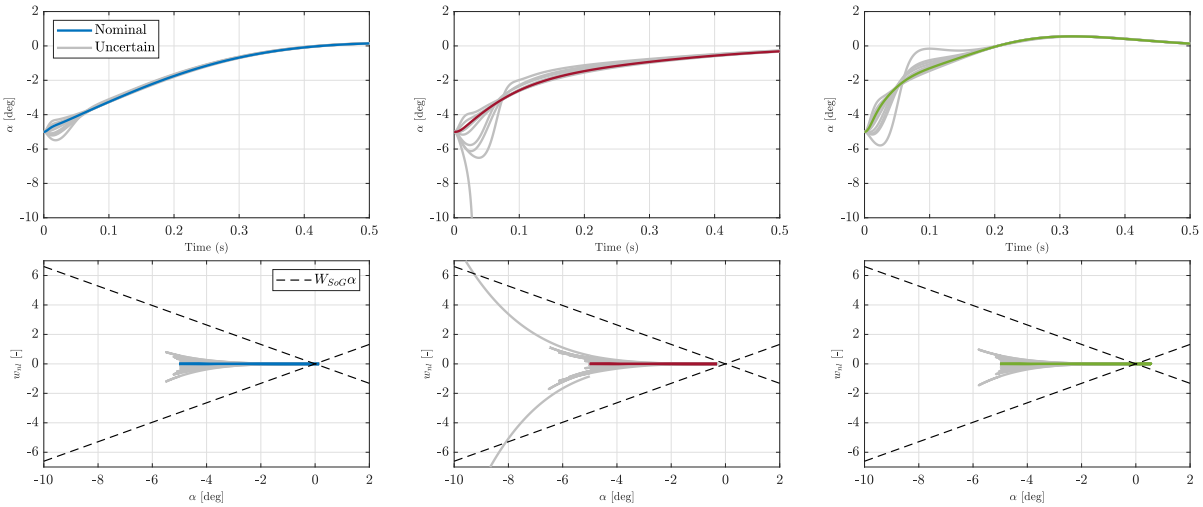

(b) Sampled stiffness offsets obtained for relative coefficient uncertainty of [50, 150, 500, 1000, 2500]%.

Fig. 11 Nonlinear sensitivity to uncertainty.

same number of controller states[‖]. Consequently, the additional structure imposed by the presented INDI controllers leads to restrictions in terms of attainable nonlinear robust stability and performance for the problem at hand.

Regarding the distinctive characteristics observed between the hybrid and sensor-based INDI alternatives, the impact of using model predictions must be further deliberated. Thanks to the embedded model, hybrid INDI is capable of fully eliminating the nominal nonlinearities associated with the plant under consideration. This is in contrast to the sensor-based alternative, which relies on a filtered version of $\boldsymbol{u}_{eq}$ to perform plant transformations. This leads to inversion distortions as a result, as discussed in Section III.A.4. In turn, the stability properties of the nominal closed-loop system are affected, which needs to be resolved through the virtual control law. This comes in addition to the other design objectives, whereas the number of design degrees of freedom remains the same as in hybrid INDI. The results in this case study show that this comes at the cost of overall performance and robustness.

On the other hand, the use of unfiltered feedback of $\boldsymbol{u}_{eq}$ as in hybrid INDI leads to other downsides. For example, model offsets induce fast transients. This relates to additional control activity and an increased likelihood of exiting the region of attraction of the closed-loop system. This shows the importance of imposing limits on the bandwidth of all control loops. Whereas this leads to inversion distortions in the INDI setup, the q-LPV controller can be designed with this aspect in mind from the onset. Similar considerations apply to stability margins at the plant output.

Finally, some remarks regarding the q-LPV controller should be made. As discussed in Section IV, the LFT-LPV synthesis strategy generally leads to a degree of conservativeness in the control design. This does not result in significant limitations for the affine LPV system in the present case study. However, the impact may become substantial for systems with more complex scheduling dependencies. This relates not only to performance and robustness, but also to nominal stability in the case of direct q-LPV controllers. With (I)NDI-based inversion, however, nominal stability is not affected

[‖]This also suggests that the number of states and tunable parameters could be reduced for the presented direct q-LPV design.

by the synthesis representation. Instead, as discussed in Section II.A, it is directly determined by the selection of the CV and the nature of the virtual control law. Therefore, as the scheduling dependency increases in complexity, (I)NDI-based control can be expected to become a more effective option.

VI. Conclusions

This paper attempts to shed new light on the performance and robustness capabilities of INDI-based control by exploiting the concepts of robust q-LPV design. Central to the insights obtained is the duality between the transforming nature of (I)NDI-based control laws and state transformations in control-oriented q-LPV modeling. Both approaches were investigated methodologically, leading to a q-LPV modeling framework for (I)NDI-based control laws that covers a broad range of inversion strategies and scenarios. This framework enables robust analysis and synthesis of (I)NDI-based control laws in an LPV sense and is applicable to any nonlinear dynamic system that falls within the class of output-nonlinear systems. Its effectiveness was demonstrated in a control design case study for a simulated nonlinear aeroservoelastic system. Here, both q-LPV and INDI-based controllers were optimized and compared in terms of robustness and performance over a wide operating range.

In summary, the following conclusions are drawn. While the aforementioned duality shows important parallels, INDI-based control imposes a particular structure on the controller in a way that deviates from the fundamental robust design principles as seen in robust (q-LPV) control. This structure may lead to restrictions in terms of attainable LPV robustness and performance. The presented design case study emphasizes this aspect, where it was shown that a direct q-LPV controller of the same order outperforms hybrid and sensor-based INDI controllers in terms of achieved robustness levels. However, the transparency and modularity benefits associated with the (I)NDI architecture can be important reasons for choosing this class of controllers in practical settings. This also connects to the typical trade-off between controller capability and complexity. The framework presented in this paper enables the configuration of (I)NDI-based controllers to achieve near-optimal q-LPV robustness levels. As a result, such trade-offs can be made effectively and systematically.

References

[1] Zhou, K., and Doyle, J., *Essentials of Robust Control*, Prentice Hall, 1998. ISBN 978-0137908745.

[2] Bates, D., and Postlethwaite, I., *Robust multivariable control of aerospace systems*, DUP Science, 2002. ISBN 978-9040723179.

[3] Skogestad, S., and Postlethwaite, I., *Multivariable Feedback Control: analysis and design*, 2nd ed., John Wiley & Sons Ltd., 2005. ISBN 978-0470011683.

[4] Megretski, A., and Rantzer, A., "System analysis via integral quadratic constraints," *IEEE Transactions on Automatic Control*, Vol. 42, No. 6, 1997, pp. 819–830. https://doi.org/10.1109/9.587335.

[5] Veenman, J., Scherer, C. W., and Köroğlu, H., "Robust stability and performance analysis based on integral quadratic constraints," *European Journal of Control*, Vol. 31, 2016, pp. 1–32. https://doi.org/10.1016/j.ejcon.2016.04.004.

[6] Rugh, W. J., and Shamma, J. S., "Research on gain scheduling," *Automatica*, Vol. 36, No. 10, 2000, pp. 1401–1425. https://doi.org/10.1016/S0005-1098(00)00058-3.

[7] Leith, D. J., and Leithead, W. E., "Survey of gain-scheduling analysis and design," *International Journal of Control*, Vol. 73, No. 11, 2000, pp. 1001–1025. https://doi.org/10.1080/002071700411304.

[8] Theodoulis, S., "Robust Control in a Nonlinear Context for Large Operating Domains," Theses, Université Paris Sud - Paris XI, Dec. 2008.

[9] Kaminer, I., Pascoal, A., Khargonekar, P., and Coleman, E., "A velocity algorithm for the implementation of gain-scheduled controllers," *Automatica*, Vol. 31, No. 8, 1995, pp. 1185–1191. https://doi.org/10.1016/0005-1098(95)00026-S.

[10] Lhachemi, H., Saussié, D., and Zhu, G., "Gain-Scheduling Control Design in the Presence of Hidden Coupling Terms," *Journal of Guidance, Control, and Dynamics*, Vol. 39, No. 8, 2016, pp. 1871–1879. https://doi.org/10.2514/1.G001830.

[11] Apkarian, P., Gahinet, P., and Becker, G., "Self-scheduled H_∞ control of linear parameter-varying systems: a design example," *Automatica*, Vol. 31, No. 9, 1995, pp. 1251–1261. https://doi.org/10.1016/0005-1098(95)00038-X.

[12] Stilwell, D. J., and Rugh, W. J., "Stability preserving interpolation methods for the synthesis of gain scheduled controllers," *Automatica*, Vol. 36, No. 5, 2000, pp. 665–671. https://doi.org/10.1016/S0005-1098(99)00193-4.

[13] Tischler, M. B., Berger, T., Ivler, C. M., Mansur, M. H., Cheung, K. K., and Soong, J. Y., *Practical methods for aircraft and rotorcraft flight control design: an optimization-based approach*, American Institute of Aeronautics and Astronautics, 2017. ISBN 978-1624104435.

[14] Shamma, J. S., "Analysis and design of gain scheduled control systems," Ph.D. thesis, Massachusetts Institute of Technology, 1988.

[15] Shamma, J. S., and Athans, M., "Guaranteed properties of gain scheduled control for linear parameter-varying plants," *Automatica*, Vol. 27, No. 3, 1991, pp. 559–564. https://doi.org/10.1016/0005-1098(91)90116-J.

[16] Apkarian, P., and Gahinet, P., "A convex characterization of gain-scheduled $\mathcal{H}_\infty$ controllers," *IEEE Transactions on Automatic Control*, Vol. 40, No. 5, 1995, pp. 853–864. https://doi.org/10.1109/9.384219.

[17] Wu, F., Yang, X. H., Packard, A., and Becker, G., "Induced L2-norm control for LPV systems with bounded parameter variation rates," *International Journal of Robust and Nonlinear Control*, Vol. 6, No. 9-10, 1996, pp. 983–998. https://doi.org/10.1002/(SICI)1099-1239(199611)6:9/10<983::AID-RNC263>3.0.CO;2-C.

[18] Marcos, A., and Balas, G. J., "Development of Linear-Parameter-Varying Models for Aircraft," *Journal of Guidance, Control, and Dynamics*, Vol. 27, No. 2, 2004, pp. 218–228. https://doi.org/10.2514/1.9165.

[19] Tóth, R., *Modeling and identification of linear parameter-varying systems*, Springer Berlin, Heidelberg, 2010. https://doi.org/10.1007/978-3-642-13812-6, ISBN 978-3642138126.

[20] Shamma, J. S., and Cloutier, J. R., "Gain-scheduled missile autopilot design using linear parameter varying transformations," *Journal of Guidance, Control, and Dynamics*, Vol. 16, No. 2, 1993, pp. 256–263. https://doi.org/10.2514/3.20997.

[21] Tan, W., Packard, A., and Balas, G., "Quasi-LPV modeling and LPV control of a generic missile," *Proceedings of the 2000 American Control Conference. ACC (IEEE Cat. No.00CH36334)*, Vol. 5, 2000, pp. 3692–3696 vol.5. https://doi.org/10.1109/ACC.2000.879259.

[22] Koelewijn, P., "Analysis and Control of Nonlinear Systems with Stability and Performance Guarantees: A Linear Parameter-Varying Approach," Ph.D. thesis, Eindhoven University of Technology, 2023. ISBN 978-9038656571.

[23] Papageorgiou, G., and Glover, K., "Design of a robust gain scheduled controller for the high incidence research model," *Guidance, Navigation, and Control Conference and Exhibit*, Portland, OR, USA, 1999. https://doi.org/10.2514/6.1999-4276, AIAA-1999-4276.

[24] Papageorgiou, G., Glover, K., D'Mello, G., and Patel, Y., "Development of a 'reliable' LPV model for the longitudinal dynamics of DERA's VAAC Harrier," American Institute of Aeronautics and Astronautics, Denver, CO, USA, 2000. https://doi.org/10.2514/6.2000-4459, AIAA 2000-4459.

[25] Papageorgiou, G., Glover, K., D'Mello, G., and Patel, Y., "Taking robust LPV control into flight on the VAAC Harrier," IEEE, Sydney, NSW, Australia, 2000. https://doi.org/10.1109/CDC.2001.914633.

[26] Vinco, G. M., "Flight Dynamics Modeling and Autopilot Design for Guided Projectiles via Linear Parameter-Varying Techniques," Theses, Université Grenoble Alpes, Feb. 2024. URL https://theses.hal.science/tel-04593695.

[27] Autenrieb, J., Fezans, N., and Gruhn, P., "A Quasi-LPV Approach for Gain Scheduling Cascaded NDI-Based Controllers for Hypersonic Glide Vehicles," *AIAA SCITECH 2025 Forum*, Orlando, FL, USA, 2025. https://doi.org/10.2514/6.2025-1908, AIAA-2025-1908.

[28] Enns, D., Bugajski, D., Hendrick, R., and Stein, G., "Dynamic inversion: an evolving methodology for flight control design," *International Journal of Control*, Vol. 59, No. 1, 1994, pp. 71–91. https://doi.org/10.1080/00207179408923070.

[29] Pollack, T., "Advances in Dynamic Inversion-based Flight Control Law Design: Multivariable Analysis and Synthesis of Robust and Multi-Objective Design Solutions," Dissertation (TU Delft), Delft University of Technology, 2024. https://doi.org/10.4233/uuid:28617ba0-461d-48ef-8437-de2aa41034ea.

[30] Wacker, R., Munday, S., and Merkle, S., "X-38 application of dynamic inversion flight control," *24th Annual Guidance and Control Conference*, American Astronautical Society, Breckenridge, CO, USA, 2001.

[31] Enns, D., and Keviczky, T., "Dynamic inversion based flight control for autonomous RMAX helicopter," *2006 American Control Conference*, IEEE, Minneapolis, MN, USA, 2006. https://doi.org/10.1109/ACC.2006.1657330.

[32] Harris, J. J., and Stanford, J. R., "F-35 Flight Control Law Design, Development and Verification," *2018 Aviation Technology, Integration, and Operations Conference*, American Institute of Aeronautics and Astronautics, Atlanta, GA, USA, 2018. https://doi.org/10.2514/6.2018-3516, AIAA-2018-3516.

[33] Sieberling, S., Chu, Q. P., and Mulder, J. A., "Robust Flight Control Using Incremental Nonlinear Dynamic Inversion and Angular Acceleration Prediction," *Journal of Guidance, Control, and Dynamics*, Vol. 33, No. 6, 2010, pp. 1732–1742. https://doi.org/10.2514/1.49978.

[34] Wang, X., van Kampen, E., Chu, Q. P., and Lu, P., "Stability Analysis for Incremental Nonlinear Dynamic Inversion Control," *Journal of Guidance, Control, and Dynamics*, Vol. 42, No. 5, 2019, pp. 1116–1129. https://doi.org/10.2514/1.G003791.

[35] Pollack, T., and van Kampen, E., "Robust Stability and Performance Analysis of Incremental Dynamic-Inversion-Based Flight Control Laws," *Journal of Guidance, Control, and Dynamics*, Vol. 46, No. 9, 2023, pp. 1785–1798. https://doi.org/10.2514/1.G006576.

[36] Kim, C.-S., Ji, C.-H., Koh, G.-O., and Kim, B. S., "Stability margin and structural coupling analysis of a hybrid INDI control for the fighter aircraft," *International Journal of Aeronautical and Space Sciences*, Vol. 22, No. 5, 2021, pp. 1154–1169. https://doi.org/10.1007/s42405-021-00394-8.

[37] Kumtepe, Y., Pollack, T., and van Kampen, E., "Flight Control Law Design using Hybrid Incremental Nonlinear Dynamic Inversion," *AIAA SciTech 2022 Forum*, American Institute of Aeronautics and Astronautics, San Diego, CA, USA & Virtual, 2022. https://doi.org/10.2514/6.2022-1597, AIAA-2022-1597.

[38] Pollack, T. S. C., Theodoulis, S. T., and van Kampen, E., "Commonalities between robust hybrid incremental nonlinear dynamic inversion and proportional-integral-derivative flight control law design," *Aerospace Science and Technology*, Vol. 152, 2024, p. 109377. https://doi.org/10.1016/j.ast.2024.109377.

[39] Pollack, T., Theodoulis, S., and Wang, X., "Quasi-LPV Transformations for Robust Gain Scheduling of Incremental Nonlinear Dynamic Inversion-based Controllers," *IFAC-PapersOnLine*, Vol. 59, No. 15, 2025, pp. 97–102. https://doi.org/10.1016/j.ifacol.2025.10.064, 6th IFAC Workshop on Linear Parameter Varying Systems LPVS 2025.

[40] Khalil, H., *Nonlinear Systems*, 3rd ed., Prentice Hall, 2002. ISBN 978-0130673893.

[41] Osterhuber, R., Hanel, M., and Hammon, R., "Realization of the Eurofighter 2000 Primary Lateral/Directional Flight Control Laws with Differential PI-Algorithm," American Institute of Aeronautics and Astronautics, Providence, RI, USA, 2004. https://doi.org/10.2514/6.2004-4751, AIAA 2004-4751.

[42] Packard, A., "Gain scheduling via linear fractional transformations," *Systems & Control Letters*, Vol. 22, No. 2, 1994, pp. 79–92. https://doi.org/10.1016/0167-6911(94)90102-3.

[43] Shamma, J., "Robust stability with time-varying structured uncertainty," *IEEE Transactions on Automatic Control*, Vol. 39, No. 4, 1994, pp. 714–724. https://doi.org/10.1109/9.286248.

[44] Desoer, C. A., and Vidyasagar, M., *Feedback Systems: Input-Output Properties*, Classics in Applied Mathematics, Society for Industrial and Applied Mathematics, 2009. https://doi.org/10.1137/1.9780898719055.

[45] Packard, A., Doyle, J., and Balas, G., "Linear, Multivariable Robust Control With a μ Perspective," *Journal of Dynamic Systems, Measurement, and Control*, Vol. 115, No. 2B, 1993, pp. 426–438. https://doi.org/10.1115/1.2899083.

[46] Apkarian, P., and Noll, D., "Nonsmooth H_∞ Synthesis," *IEEE Transactions on Automatic Control*, Vol. 51, No. 1, 2006, pp. 71–86. https://doi.org/10.1109/TAC.2005.860290.

[47] Apkarian, P., and Noll, D., "The H_∞ Control Problem is Solved," *Aerospace Lab*, , No. 13, 2017, pp. pages 1–11. https://doi.org/10.12762/2017.AL13-01.

[48] Anonymous, *Control System Toolbox™ Reference*, The MathWorks, Inc., 2024.

[49] Barker, J. M., and Balas, G. J., "Comparing Linear Parameter-Varying Gain-Scheduled Control Techniques for Active Flutter Suppression," *Journal of Guidance, Control, and Dynamics*, Vol. 23, No. 5, 2000, pp. 948–955. https://doi.org/10.2514/2.4637.

[50] Ko, J., Kurdila, A. J., and Strganac, T. W., "Nonlinear Control of a Prototypical Wing Section with Torsional Nonlinearity," *Journal of Guidance, Control, and Dynamics*, Vol. 20, No. 6, 1997, pp. 1181–1189. https://doi.org/10.2514/2.4174.

[51] Lhachemi, H., Chu, Y., Saussié, D., and Zhu, G., "Flutter Suppression for Underactuated Aeroelastic Wing Section: Nonlinear Gain-Scheduling Approach," *Journal of Guidance, Control, and Dynamics*, Vol. 40, No. 8, 2017, pp. 2102–2109. https://doi.org/10.2514/1.G002497.

[52] Sun, B., Wang, X., and van Kampen, E., "Event-triggered intelligent critic control with input constraints applied to a nonlinear aeroelastic system," *Aerospace Science and Technology*, Vol. 120, 2022, p. 107279. https://doi.org/10.1016/j.ast.2021.107279.

[53] Hjartarson, A., Seiler, P., and Packard, A., "LPVTools: A Toolbox for Modeling, Analysis, and Synthesis of Parameter Varying Control Systems," *IFAC-PapersOnLine*, Vol. 48, No. 26, 2015, pp. 139–145. https://doi.org/10.1016/j.ifacol.2015.11.127, 1st IFAC Workshop on Linear Parameter Varying Systems LPVS 2015.

A. Additional Derivations for (I)NDI-based q-LPV Modeling with Singular Perturbations

In this Appendix, it is shown how the q-LPV representation from Section III.A.3 can be constructed. To construct the singular perturbation model, a change of variables is adopted [40]. In particular, setting $\epsilon = 0$ and recognizing that $\boldsymbol{w}_{dev} = \boldsymbol{0}$ and $\tilde{\boldsymbol{e}}_\xi = \boldsymbol{0}$ in equilibrium allows one to find the isolated real roots of $\boldsymbol{\phi}$ as:

$$\boldsymbol{\phi}_r = \boldsymbol{u}_{eq}(z) = -B_2^{-1}(z)\left[\boldsymbol{k}_2(z) + A_{21}(z)z + A_{22}(z)\boldsymbol{w}_{eq}\right] \tag{64}$$

Consequently, the change of variable $\boldsymbol{\psi} \triangleq \boldsymbol{\phi} - \boldsymbol{\phi}_r$ is employed. As a result, Equation 38 can be rewritten as

$$\boldsymbol{u} = B_2^{-1}(z)\boldsymbol{\nu} + \boldsymbol{\psi} + \boldsymbol{u}_{eq}(z) \tag{65}$$

with

$$\epsilon\dot{\boldsymbol{\psi}} = \epsilon\left(\dot{\boldsymbol{\phi}} - \dot{\boldsymbol{\phi}}_r\right) = -\boldsymbol{\psi} - B_2^{-1}(z)\left[A_{22}(z)\boldsymbol{w}_{dev} + K_c(z)\tilde{\boldsymbol{e}}_\xi\right] - \epsilon\frac{\partial \boldsymbol{u}_{eq}(z)}{\partial z}\dot{z} \tag{66}$$

Subsequent application of the approximate inversion law from Eq. 38 to the system in Eq. 12 yields:

$$\begin{bmatrix}\dot{z}\\ \dot{\boldsymbol{w}}\\ \epsilon\dot{\boldsymbol{\psi}}\end{bmatrix} = \begin{bmatrix}\boldsymbol{k}_1^*(z)\\ 0\\ -\epsilon\frac{\partial \boldsymbol{u}_{eq}(z)}{\partial z}\boldsymbol{k}_1^*(z)\end{bmatrix} + \begin{bmatrix}A_{11}^*(z) & A_{12}^*(z) & B_1(z)\\ 0 & 0 & B_2(z)\\ -\epsilon\frac{\partial \boldsymbol{u}_{eq}(z)}{\partial z}A_{11}^*(z) & -\epsilon\frac{\partial \boldsymbol{u}_{eq}(z)}{\partial z}A_{12}^*(z) & -I - \epsilon\frac{\partial \boldsymbol{u}_{eq}(z)}{\partial z}B_1(z)\end{bmatrix}\begin{bmatrix}z\\ \boldsymbol{w}\\ \boldsymbol{\psi}\end{bmatrix} + \begin{bmatrix}B_1^*(z)A_{22}(z)\\ A_{22}(z)\\ -B_2^{-1}(z)A_{22}(z)\end{bmatrix}\boldsymbol{w}_{dev} - \begin{bmatrix}0\\ 0\\ B_2^{-1}(z)\end{bmatrix}K_c(z)\tilde{\boldsymbol{e}}_\xi + \begin{bmatrix}B_1^*(z)\\ I\\ -\epsilon\frac{\partial \boldsymbol{u}_{eq}(z)}{\partial z}B_1^*(z)\end{bmatrix}\boldsymbol{\nu} \tag{67}$$

At the equilibrium manifold, the following condition holds:

$$\begin{bmatrix}0\\ 0\\ 0\end{bmatrix} = \begin{bmatrix}\boldsymbol{k}_1^*(z)\\ 0\\ -\epsilon\frac{\partial \boldsymbol{u}_{eq}(z)}{\partial z}\boldsymbol{k}_1^*(z)\end{bmatrix} + \begin{bmatrix}A_{11}^*(z) & A_{12}^*(z) & B_1(z)\\ 0 & 0 & B_2(z)\\ -\epsilon\frac{\partial \boldsymbol{u}_{eq}(z)}{\partial z}A_{11}^*(z) & -\epsilon\frac{\partial \boldsymbol{u}_{eq}(z)}{\partial z}A_{12}^*(z) & -I - \epsilon\frac{\partial \boldsymbol{u}_{eq}(z)}{\partial z}B_1(z)\end{bmatrix}\begin{bmatrix}z\\ \boldsymbol{w}_{eq}(z)\\ 0\end{bmatrix} \tag{68}$$

Subtraction of the resulting trim map $\boldsymbol{w}_{eq}(z)$ results in:

$$\begin{bmatrix}\dot{z}\\ \dot{\boldsymbol{w}}\\ \epsilon\dot{\boldsymbol{\psi}}\end{bmatrix} = \begin{bmatrix}0 & A_{12}(z) & B_1(z)\\ 0 & A_{22}(z) & B_2(z)\\ 0 & -\epsilon\frac{\partial \boldsymbol{u}_{eq}(z)}{\partial z}A_{12}^*(z) - B_2^{-1}(z)A_{22}(z) & -I - \epsilon\frac{\partial \boldsymbol{u}_{eq}(z)}{\partial z}B_1(z)\end{bmatrix}\begin{bmatrix}z\\ \boldsymbol{w}_{dev}\\ \boldsymbol{\psi}\end{bmatrix} - \begin{bmatrix}0\\ 0\\ B_2^{-1}(z)\end{bmatrix}K_c(z)\tilde{\boldsymbol{e}}_\xi + \begin{bmatrix}B_1^*(z)\\ I\\ -\epsilon\frac{\partial \boldsymbol{u}_{eq}(z)}{\partial z}B_1^*(z)\end{bmatrix}\boldsymbol{\nu} \tag{69}$$

Then, the state transformation procedure is completed as:

$$\begin{bmatrix} \dot{\boldsymbol{z}} \\ \dot{\boldsymbol{w}}_{dev} \\ \epsilon\dot{\boldsymbol{\psi}} \end{bmatrix} = \begin{bmatrix} 0 & A_{12}(z) & B_1(z) \\ 0 & A_{22}(z) - \frac{\partial w_{eq}(z)}{\partial z} A_{12}(z) & B_2(z) - \frac{\partial w_{eq}(z)}{\partial z} B_1(z) \\ 0 & -B_2^{-1}(z)A_{22}(z) - \epsilon \frac{\partial \boldsymbol{u}_{eq}(z)}{\partial z} A_{12}^*(z) & -I - \epsilon \frac{\partial \boldsymbol{u}_{eq}(z)}{\partial z} B_1(z) \end{bmatrix} \begin{bmatrix} \boldsymbol{z} \\ \boldsymbol{w}_{dev} \\ \boldsymbol{\psi} \end{bmatrix} - \begin{bmatrix} 0 \\ 0 \\ B_2^{-1}(z) \end{bmatrix} K_c(z)\tilde{e}_\xi + \begin{bmatrix} B_1^*(z) \\ I - \frac{\partial w_{eq}(z)}{\partial z} B_1^*(z) \\ -\epsilon \frac{\partial \boldsymbol{u}_{eq}(z)}{\partial z} B_1^*(z) \end{bmatrix} \boldsymbol{\nu} \quad (70)$$

Finally, applying input augmentation and incorporating the inversion error filter dynamics yields the formulation:

$$\begin{bmatrix} \dot{\boldsymbol{z}} \\ \dot{\boldsymbol{w}}_{dev} \\ \dot{\boldsymbol{u}}_{eq} \\ \dot{\tilde{\boldsymbol{e}}}_\xi \\ \epsilon\dot{\boldsymbol{\phi}} \end{bmatrix} = \begin{bmatrix} 0 & A_{12}(z) & -B_1(z) & 0 & B_1(z) \\ 0 & A_{22}(z) - \frac{\partial w_{eq}(z)}{\partial z} A_{12}(z) & -B_2(z) + \frac{\partial w_{eq}(z)}{\partial z} B_1(z) & 0 & B_2(z) - \frac{\partial w_{eq}(z)}{\partial z} B_1(z) \\ 0 & \frac{\partial \boldsymbol{u}_{eq}(z)}{\partial z} A_{12}(z) & -\frac{\partial \boldsymbol{u}_{eq}(z)}{\partial z} B_1(z) & 0 & \frac{\partial \boldsymbol{u}_{eq}(z)}{\partial z} B_1(z) \\ 0 & 0 & 0 & -A_c(z) & 0 \\ 0 & -B_2^{-1}(z)A_{22}(z) & I & -B_2^{-1}(z)K_c(z) & -I \end{bmatrix} \begin{bmatrix} \boldsymbol{z} \\ \boldsymbol{w}_{dev} \\ \boldsymbol{u}_{eq} \\ \tilde{\boldsymbol{e}}_\xi \\ \boldsymbol{\phi} \end{bmatrix} + \begin{bmatrix} B_1^*(z) \\ I - \frac{\partial w_{eq}(z)}{\partial z} B_1^*(z) \\ \frac{\partial \boldsymbol{u}_{eq}(z)}{\partial z} B_1^*(z) \\ 0 \\ 0 \end{bmatrix} \boldsymbol{\nu} + \begin{bmatrix} 0 \\ B_2(z) \\ 0 \\ B_c(z)B_2(z) \\ 0 \end{bmatrix} \boldsymbol{d}_i \quad (71)$$

which is the result from Equation 39. Here, the relation $\boldsymbol{\phi} = \boldsymbol{\psi} + \boldsymbol{u}_{eq}$ has been used to transform back to the original filtered input state.